

Pulse-number distribution for the neural spike train in the cat's auditory nerve

Malvin C. Teich and Shyam M. Khanna

Department of Electrical Engineering, Columbia University, New York, New York 10027 and Fowler Memorial Laboratory, Department of Otolaryngology, Columbia College of Physicians and Surgeons, New York, New York 10032

(Received 31 October 1983; accepted for publication 2 November 1984)

Pulse-number distributions (PNDs) were recorded from primary afferent fibers in the auditory nerve of the cat, using standard extracellular microelectrode recording techniques. Pure-tone and broadband-noise stimuli were used. The number of neural spikes (pulses) n was measured in a set of contiguous intervals, each of duration T seconds. The quantity n varies from one interval to another. These data were then used to determine the PND, which is the probability $p(n, T)$ of occurrence of n spikes in the time T , versus the number n . The estimated mean and variance of $p(n, T)$ were obtained. Two different values of T were used. An unexpected observation was that the count mean-to-variance ratio R is relatively constant and independent of the stimulus intensity. Use of the PND as a statistical measure of the underlying neural point process has a number of virtues. For example, the PND readily exhibits the existence of spike clusters (e.g., pairs) for some units. The PND is essentially unaffected by time jitter and time quantization and provides a statistically significant measure for units firing at low rates. A study of the scaled and unscaled pulse-interval distributions (PIDs), under conditions of spontaneous firing, demonstrates that the occurrences of neural events are generally not describable by a renewal process. Our investigation shows that none of the point processes customarily used to model the auditory neural spike train is consistent with all of the data. It appears that the encoding of acoustic information into nerve spikes in the peripheral auditory system takes the form of a cluster point process similar to the Neyman-Scott type. For pure-tone excitation, the PND will be well represented as a multinomial distribution in this case.

PACS numbers: 43.63.Pd, 43.63.Th

INTRODUCTION

It is well known that in mammals, the pathway for the transfer of information from the inner ear to higher auditory centers in the brain is provided by the VIIIth nerve. The neural signal transmitted on individual fibers of this nerve has been studied by many researchers, with the goal of gaining insight into the mechanisms of information encoding (Galambos and Davis, 1943, 1948; Tasaki, 1954; Katsuki *et al.*, 1958; Kiang *et al.*, 1962, 1965; Rose *et al.*, 1967, 1971; Hind *et al.*, 1967; Evans, 1972, 1975; Kiang, 1984). This signal is comprised of a series of brief electrical nerve spikes, whose amplitude and energy are widely assumed not to be significant variables. Rather, it is generally accepted that the times of occurrences of the spikes carry the auditory information [indeed, early "telephone" theories of hearing, such as that of Rutherford (1886), were structured along these lines]. There is an element of randomness involved in the encoding scheme, since ensembles of identical single-fiber experiments lead to differing sequences of nerve spikes (Tasaki, 1954; Peake *et al.*, 1962; Rupert *et al.*, 1963; Kiang, 1984).

From a mathematical point of view, the neural activity in a peripheral auditory fiber is perhaps best characterized as an (unmarked) stochastic point process (Parzen, 1962; Cox and Lewis, 1966; Moore *et al.*, 1966; Perkel *et al.*, 1967; Fienberg, 1974; Lewis, 1972; Snyder, 1975; Holden, 1976; Lan-

dolt and Correia, 1978; Cox and Isham, 1980; de Kwaadsteniet, 1982). The term "point process" designates a sequence of events with localized times of occurrence; the modifier "unmarked" signifies that all individual events comprising the process are taken to be identical. Probably the simplest and most widely occurring stochastic point process is the one-dimensional homogeneous Poisson process (Parzen, 1962; Haight, 1967). It plays the role that the Gaussian plays in the theory of continuous stochastic processes. The homogeneous Poisson point process (HPP) is characterized by a single quantity, its rate, which is constant. Its distinguishing feature is that it evolves in time without after-effects. This means that the occurrence times and number of events before an arbitrary time have no bearing on the subsequent occurrence times and numbers of events. It is said to have zero memory. However, rarely does the HPP describe the behavior of an actual neural spike train.

A more common (and superior) description is provided by the renewal point process (RPP), in which the successive time intervals between adjacent events are drawn independently from a common probability distribution (Cox, 1962). [The RPP derives its name from the application for which it was developed: the replacement (renewal) of industrial components. The HPP is a special case of the RPP.] Nevertheless a good deal of neural spike-train data does not satisfy the conditions of the RPP either (Hyvärinen, 1966). As a result,

more complex point processes, differing substantially from the RPP, have been proposed as stochastic models for spike-train data (Pecher, 1939; Verveen, 1961; Ten Hoopen *et al.*, 1963; Gerstein and Mandelbrot, 1964; Weiss, 1966; McGill, 1967; Siebert, 1968; Ekholm and Hyvärinen, 1970; Ekholm, 1972; Teich and McGill, 1976). Some of these are based on presumed physiological mechanisms, such as the level crossings of a continuous "summation" signal, whereas others are set forth on a more *ad hoc* basis. There are many point processes that can explain one or another feature of the data; the problem is one of uniqueness.

Identifying a point process is not an easy task. Given a set of experimental data, one of the more productive approaches to carrying this out is to simultaneously sort the data in a number of different ways that emphasize one or another of its features. There are many such ways. In practice, it is often useful to synthesize a process that is consistent with as many features of the data as possible, so as to narrow the field of candidates.

The feature that is the most widely used in neurophysiology is the interspike-interval or pulse-interval distribution (PID). It appears to have been first employed by Brink *et al.* (1946) and by Hagiwara (1954). More recently, Kuffler *et al.* (1957) measured the PID in a seminal study of the maintained discharge in the cat's retinal ganglion cell. The PID was introduced to auditory neurophysiology [specifically for recordings from the cochlear nucleus (CN) and auditory cortex] by Gerstein and Kiang (1960). The joint and scaled-interval histograms, which are generalizations of the PID, were examined (in the case of spontaneous activity in CN units) by Rodieck *et al.* (1962).

The data can also be sorted into the pulse-number distribution (PND). This is one of the more common measures used in many branches of probability, but not very often in neurophysiology. Poisson, for example, employed the PND in the 19th century for many applications. In modern times, it has been used to describe the registration of nuclear particles (Rutherford and Geiger, 1910; Müller, 1973, 1974) as well as the detection of optical photons (Einstein, 1909; Mandel, 1959; Saleh, 1978; Teich *et al.*, 1984). In the life sciences, the PND has been used as a theoretical construct in visual psychophysics (Hecht *et al.*, 1942; Teich *et al.*, 1982), and in auditory psychophysics (McGill, 1967; Siebert, 1968; Teich and McGill, 1976; Teich and Lachs, 1979). Its first use in sensory neurophysiology appears to be in the studies carried out by Barlow and Levick (1969a,b) and Barlow *et al.* (1971) on the neural discharge in the retinal ganglion cell of the cat. The experimental work presented here represents, as far as we know, the first measurement of the PND in auditory neurophysiology.

Perhaps the easiest way to illustrate the different views of the underlying point process offered by the PND and PID is provided in Fig. 1. In Fig. 1(a), we schematically illustrate five samples records of idealized neural spikes from a peripheral auditory fiber. The parameter T is a fixed time interval (counting time) during which a count of the number of nerve impulses (n) is taken in each record; in the above illustration, n is equal to 3, 7, 4, 6, and 4 impulses (or counts) in the five records. The time interval between two adjacent im-

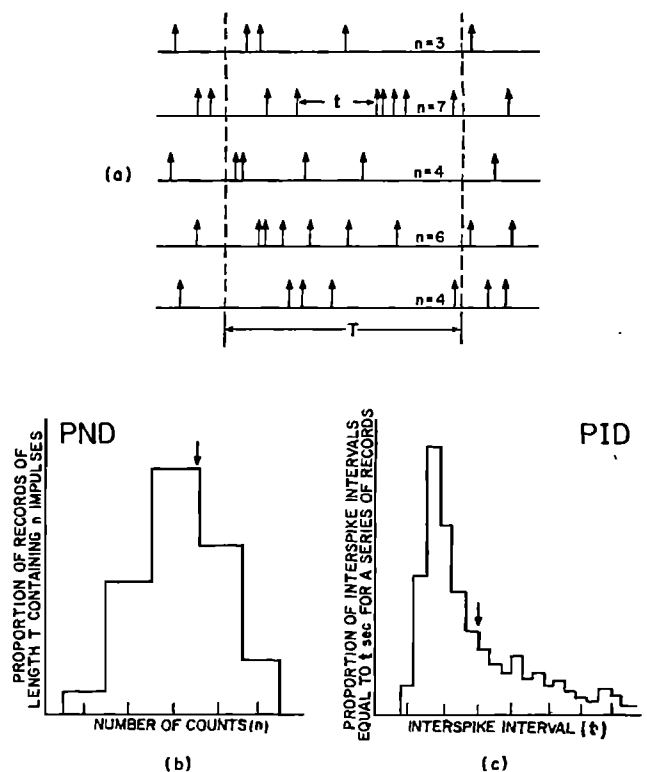


FIG. 1. (a) Five sample records of idealized neural spikes from a peripheral auditory fiber are schematized. T is the fixed time interval (counting time) during which a count of the number of nerve impulses (n) is taken in each record; $n = 3, 7, 4, 6,$ and 4 impulses (or counts) in the five records. The time interval between two adjacent impulses in the second record (t) represents the (random) interspike interval. (b) Pulse-number distribution (PND) or counting distribution. Arrow indicates mean number of counts. (c) Pulse-interval distribution (PID) or interspike-interval distribution. Allowed values of t are quantized, either for convenience or as a result of the finite time resolution of the instrument. Arrow indicates mean interspike time interval. [The PND shown in (b) and the PID shown in (c) are illustrative, and were not drawn from the records in (a).]

pulses in the second record, labeled t , represents the (random) interspike interval. The pulse-number distribution (PND) or counting distribution is shown in Fig. 1(b). It is a relative frequency distribution of the number of counts n over a set of experimental records such as those illustrated in Fig. 1(a). The ordinate represents the proportion of the total number of records for which the value of n on the abscissa was obtained. The arrow indicates the mean number of counts. The pulse-interval distribution (PID) or interspike-interval distribution is presented in Fig. 1(c). It is a relative frequency distribution of the number of interspike intervals t over a set of sample records such as those illustrated in Fig. 1(a). The ordinate represents the proportion of the total number of records for which the value of t on the abscissa was obtained. The allowed values of t are quantized, either for convenience or as a result of the finite time resolution of the instrument. The arrow indicates the mean interspike time interval. [The PND shown in Fig. 1(b) and the PID shown in Fig. 1(c) are illustrative, and were not drawn from the records in Fig. 1(a).] For the HPP, the PND is the Poisson counting distribution, and the PID is the exponential interspike-interval distribution (Cox, 1962).

We have pointed out that both the PID and the PND are useful and commonly used measures of a point process. A number of authors have used the experimentally measured PID in the CN (Gerstein and Kiang, 1960; Rodieck *et al.*, 1962; Gerstein and Mandelbrot, 1964), and in primary VIIIth nerve fibers (Kiang *et al.*, 1965; Walsh *et al.*, 1972), to show that spontaneous and driven auditory neural activity is not well represented as a HPP. Using experimentally measured PNDs, we will also demonstrate, but from a different point of view, that the point process in the primary fibers cannot be a HPP. More significantly, however, it will become apparent from our study that the PID and PND provide different kinds of information about the details of the spike occurrences. Indeed, the two data are complementary, and should be used together to provide a more complete understanding of the underlying coding mechanism.

What are some of the differences in the information provided by each? Inasmuch as the PID is a histogram formed from successive events, it has a principal time scale of the order of the interspike interval which is internal to the point process. The PND, on the other hand, records all events within the externally determined counting time T , which therefore plays a role in its behavior. As one example of the distinction provided by the two measures, consider a cluster of a few neural spikes whose relative spacing is variable from trial to trial, but all of which repeatedly occur within a time short in comparison with the counting time T . Because of the interspike variability, the relationship between spikes in the cluster may not be evident in the PID. But the cluster as a whole would be repeatedly captured in certain trials of the PND, and its presence would therefore be evident. As an example of this, we will see that neural spike pairs appear quite prominently in our experimental PND data. In principal, if an experimental set of PNDs with different values of T is available, it can be related to PID data, but the usefulness and accuracy of these relations is seriously limited in practice (Gundersdorf, 1971).

There are measures of a point process, other than the PIDs, that are based on a time marker provided by the occurrence of an event. The spike-discharge probability, conditioned on the occurrence of a spike, has been used by Gray (1967) and more recently by Gaumond *et al.* (1982). This measure can elucidate the relatively long-lasting effects of (relative) refractoriness in terms of a recovery function. Ruggero (1973) has effectively used the PID, together with a similarly triggered measure called the autocorrelogram, to analyze the time structure of the neural response to noise. The correlation function and spectrum of the point process are also sometimes studied.

There are yet other ways of characterizing the statistical behavior of the underlying neural-event point process. The most celebrated of these is the post-stimulus time histogram (PST) (Gerstein and Kiang, 1960; Kiang *et al.*, 1965; Rose *et al.*, 1967), which is based on a time marker provided by the stimulus itself rather than by the occurrence of an event. PST histograms synchronized to individual cycles of the stimulus tone are called period histograms (PH) and have been studied in detail by Johnson (1980). Estimates for both the instantaneous rate of the point process and the synchro-

nization index (SI) can be obtained from the PST or from the PH. The SI provides a simple, useful measure of the strength of phase locking (preferential occurrences of neural events for restricted regions of the stimulus phase). It has been investigated by Johnson (1980) for primary auditory fibers [see also Goldberg and Brown (1969), Littlefield *et al.* (1972), Littlefield (1973), and Anderson (1973)].

The PST and PH are constructed on the basis of a time marker provided by the stimulus. This is to be contrasted with the internal time marker (occurrence of an event) used for generating the PID, the recovery function, and the autocorrelogram. The PND, in its usual form, is generated by an external time marker related neither to the stimulus nor to the occurrence of an event. [However, there is a version of the PND (which we have not used here) in which the counting interval commences with the occurrence of an event. This is called the triggered PND (Saleh, 1978).]

A few words are in order about the characteristic time scales of the various measures discussed above. For the PST and PH, it is that of a stimulus unit cell, because the results are averaged modulo this time. For the PID, it is the interspike interval. For the recovery function, it is the joint two-spike characteristic time of the process (e.g., relative refractoriness), whereas for the noise-stimulated autocorrelogram, it appears to be the characteristic (natural decay) time of the auditory system. For a steady-state stimulus, the PND characteristic time is the internal correlation time of the point process, as delimited by the externally determined adjustable counting time. There may be several characteristic times that enter the PND.

All the measures discussed above involve averaging of the data. This means that performing computations to emphasize certain aspects of the spike train generally results in a loss of information about other aspects of the spike train (Gerstein and Kiang, 1960). One obvious example is the loss of detail about the time between events when measuring the PND. A complementary example is the disappearance of noncontiguous-event relationships in the PID [the serial correlation coefficient may be useful for emphasizing this particular aspect of the data, however; see Kuffler *et al.* (1957)]. Of course a simple feature like the average spike rate may be extracted from any number of measures, including the PID, PST, and PND. Needless to say, nonstationary time variations of the signal should be arduously avoided, so as not to contaminate the data. Noise and instrumental effects provide another source of information loss. Johnson (1978) considered the measurement limitations on the PID and PST imposed by time jitter (arising from threshold detection in the presence of noise), and by instrumental time quantization.

One of the advantages of using the PND for compiling neural data is that such time jitter and time quantization become unimportant (when the counting time T is large in comparison with the uncertainties). This affords us an opportunity to examine the neural signal in a fresh way (Teich and Khanna, 1982, 1983). As an example, we can search for synchrony at high stimulus frequencies, where it could conceivably be washed out by instrumental effects in the PST (Johnson, 1978, 1980). Strong synchrony will increase the

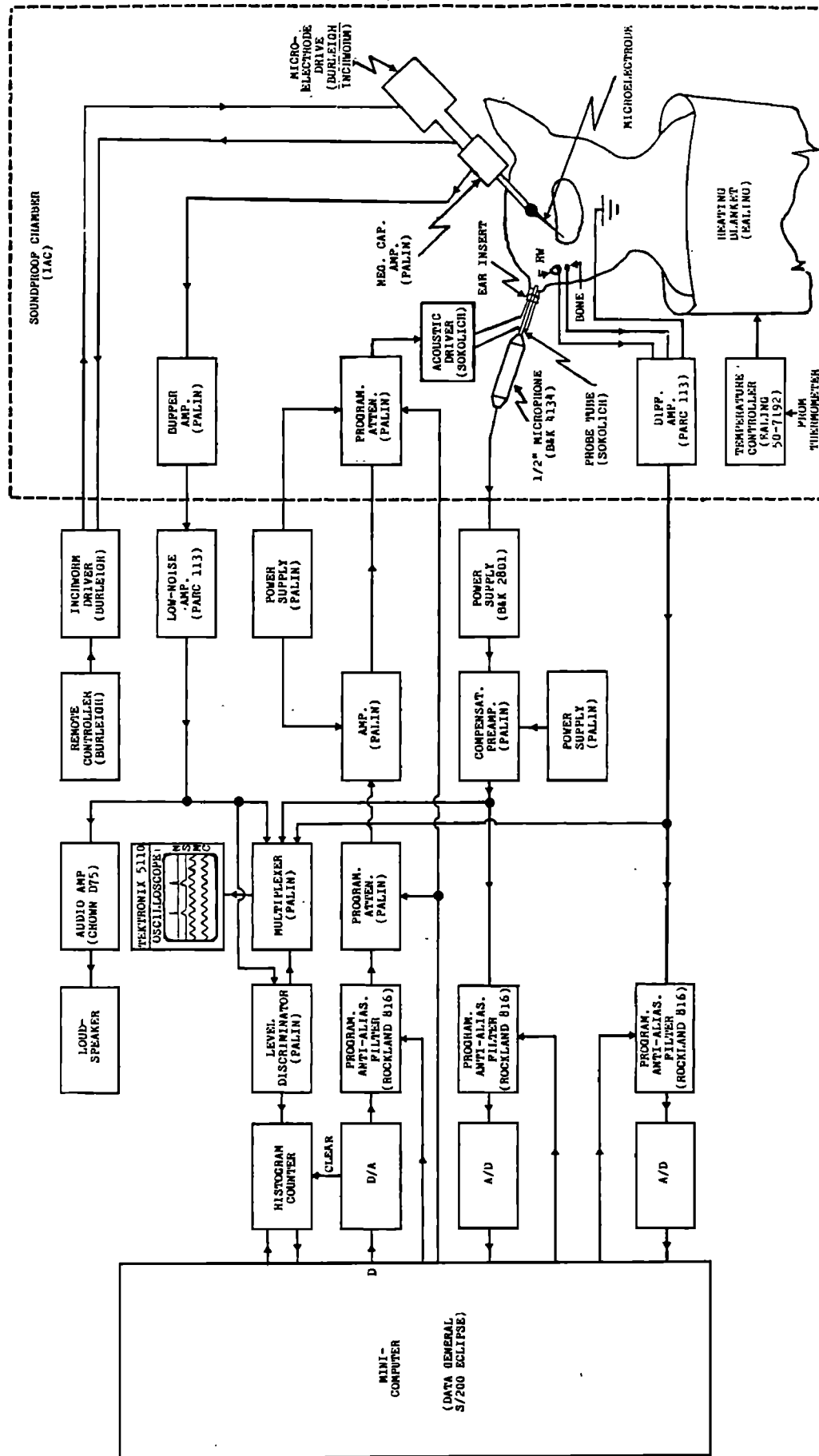


FIG. 2. Block diagram of the experimental apparatus. All digital acoustic signal generation (denoted D) and data collection were carried out with a 16-bit Data General S/200 Eclipse minicomputer.

mean-to-variance ratio of the PND, as explained in Sec. III. A further advantage of the PND is that it provides a statistically significant measure even for units firing at low rates (when the PID is very difficult to construct in a reasonable amount of time).

I. METHODS

A block diagram of the apparatus used in the experiments is shown in Fig. 2. The experimental animal (cat) is placed in an IAC double-walled soundproof chamber (large dotted box). Signal generation and data collection are carried out with a 16-bit Data General S/200 Eclipse minicomputer (leftmost box), running with the Data General Real-Time Disk Operating System (RDOS). The computer methods are the same as those used by Allen (1983). Details of the surgical preparation, acoustic signal generation, analog signal detection and processing, and neural signal detection and processing are presented in Appendices A–D, respectively.

After acquisition of a single auditory nerve fiber, and determination of its rate frequency tuning curve (FTC), a variety of nerve-spike measurements were carried out. Since our objective was to measure the steady-state neural response, data acquisition was delayed by 512 ms after the auditory signal was applied. This allowed the unit to settle down to a more-or-less stationary response pattern.

A. Construction of the experimental PST, PNDs, and PIDs

For a given stimulus frequency and sound pressure level (SPL), the PST and PNDs are simultaneously constructed from N_T identical and contiguous repetitions of the stimulus. After ten playouts of the D/A to achieve the steady-state behavior of the unit as discussed above, the histogram hardware is activated. During each subsequent playout of the D/A (which requires $25 \mu\text{s}/\text{bin} \times 2048 \text{ bins} = 51.2 \text{ ms}$) the spike occurrence times, as well as the number of spikes n , are recorded by the real-time hardware. The discretized occurrence times are transferred to an integer array of 2048 bins (denoted IHIST). The spike number n augments (by unity) the n th bin of another integer array of 25 bins (denoted IPN). After N_T repetitions, IHIST contains the PST, and IPN contains the unnormalized PND for $T = 51.2 \text{ ms}$. Both are constructed from the same sample function of the point process. Strictly speaking, the PND is not absolutely asynchronous because the beginning of the counting interval is related to the phase of the stimulus. This has little practical effect, however, since the counting time T is much longer than the period of even the lowest frequency stimulus. A second PND, for which the counting time is four times as long ($T = 204.8 \text{ ms}$), is simultaneously formed from the same data. This is accomplished by accumulating the number of spikes recorded during four contiguous playouts of the D/A before augmenting a third integer array, designated IPN4 (which has 100 bins).

The contents of the IPN array are normalized to provide the PND, denoted $p(n, T)$, in accordance with

$$p(n, T) = G(n) / \sum_{n=0}^{n_{\max}} G(n), \quad (1)$$

where $G(n)$ represents the number of times the IPN bin associated with n events has been augmented. We have chosen $n_{\max} = 25$; this is sufficiently large since there are always fewer than 25 counts in 50 ms (this corresponds to a spike rate of 500 counts/s). The distribution $p(n, T = 51.2 \text{ ms})$ is written on disk for this stimulus, as is the normalized version of IPN4, denoted $p(n, T = 204.8 \text{ ms})$. We also perform a FFT on the PST histogram, and write the amplitude and phase information for the first five Fourier components of the stimulus frequency on disk. The results of the long-time PND and PST studies will be presented elsewhere.

The normalized PID [denoted $P^{(1)}(t)$] is recorded only under undriven (spontaneous firing) conditions. For this paradigm, each time the real-time hardware records a spike, the histogram counter is reset and the time interval from the previous spike is recorded in a 2048-bin array. Data are collected for 102.4 s. The same procedure is followed for the twofold scaled PID [denoted $P^{(2)}(t)$], which is collected after (rather than simultaneously with) the ordinary PID. The twofold scaled PID is the histogram of the time intervals between *every other* spike. It is a special case of the joint PID (Rodieck *et al.*, 1962). The two PIDs are normalized and recorded on disk.

B. Statistics of the PNDs and PIDs

The experimental count mean $\bar{n}(T)$ and count variance $\sigma^2(T)$ of the PNDs are calculated from the standard formulas

$$\bar{n}(T) = \sum_{n=0}^{n_{\max}} n p(n, T), \quad (2)$$

$$\sigma^2(T) = \sum_{n=0}^{n_{\max}} n^2 p(n, T) - \left(\sum_{n=0}^{n_{\max}} n p(n, T) \right)^2, \quad (3)$$

where $n_{\max} = 25$. The mean-to-variance ratio $R(T)$ is defined as

$$R(T) \equiv \bar{n}(T) / \sigma^2(T) = 1/F(T), \quad (4)$$

where $F(T)$ is known as the index of dispersion (Cox and Isham, 1980) or the Fano factor (Teich *et al.*, 1984). For a Poisson process, $\sigma^2(T) = \bar{n}(T)$ for all T , so that $R(T) = 1$. The mean-to-variance ratio provides a simple measure for the deviation of a counting distribution from the zero-memory Poisson. As such, $R(T)$ reflects the regularity of the underlying neural spike train. This will be discussed in detail in Sec. III A.

The standard deviation of the estimator $\bar{n}(T)$, due to the finite number of samples N_T , is given approximately by (see Saleh, 1978)

$$\Delta \bar{n}(T) \simeq [\sigma^2(T)/N_T]^{1/2} = [\bar{n}(T)/R(T)N_T]^{1/2}. \quad (5)$$

For $T = 51.2 \text{ ms}$, we have found that $\bar{n}(T) \sim 5$, $R(T) \sim 1.5$, and $N_T = 1000$ so that $\Delta \bar{n}(T) \simeq 0.06$. For $T = 204.8 \text{ ms}$, on the other hand, we have $\bar{n}(T) \sim 20$, $R(T) \sim 1.0$, and $N_T = 250$, so that $\Delta \bar{n}(T) \simeq 0.28$. For a Poisson distribution (with

N_T sufficiently large), the standard deviation of $R(T)$ is calculated to be

$$\Delta R(T) \sim (2/N_T)^{1/2}. \quad (6)$$

For $T = 51.2$ ms, $N_T = 1000$ so that $\Delta R(T) \approx 0.04$. For $T = 204.8$ ms, $N_T = 250$ and therefore $\Delta R(T) \approx 0.09$. We have verified the validity of these formulas by carrying out a series of photon-counting experiments in which the parameters were chosen to be the same as those for the neural-counting experiments. These numbers will provide reasonable order-of-magnitude estimates for the errors in our statistics, even though the PNDs are not Poisson distributed. It is interesting to note that $\Delta R(T)$ is approximately independent of $\bar{n}(T)$, so that the PND can provide an accurate measure of the regularity of the neural spike train even for units firing at very low rates.

For the PIDs, the experimental mean time interval \bar{t} and interspike-interval standard deviation σ , are determined by the formulas

$$\bar{t}^{(j)} = \sum_{t=0}^{t_{\max}} t P^{(j)}(t), \quad j = 1, 2, \quad (7)$$

$$\sigma_t^{(j)} = \left[\sum_{t=0}^{t_{\max}} t^2 P^{(j)}(t) - \left(\sum_{t=0}^{t_{\max}} t P^{(j)}(t) \right)^2 \right]^{1/2}, \quad j = 1, 2, \quad (8)$$

where the interspike interval t is quantized to $25 \mu\text{s}$ (the bin width), $t_{\max} = 25 \mu\text{s}/\text{bin} \times 2048 \text{ bins} = 51.2$ ms, and $j = 1, 2$ correspond to the unscaled (ordinary) and twofold scaled PIDs, respectively. The measured values of $\bar{t}^{(j)}$ and $\sigma_t^{(j)}$ will underestimate the true values because interevent times > 51.2 ms are ignored. Thus we expect to find that $\bar{t}^{(j)} < T/\bar{n}(T)$. The coefficient of variation $CV^{(j)}$ is defined as

$$CV^{(j)} = \sigma_t^{(j)} / \bar{t}^{(j)}, \quad j = 1, 2. \quad (9)$$

$CV^{(1)}$ plays the role for the PID that $F(T) = 1/R(T)$ plays for the PND (Cox and Isham, 1980). Both carry information about the regularity of the underlying point process.

C. Sequence of measurements

The following sets of measurements were carried out. (i) For spontaneous activity, no signal was applied and the two PNDs, the PID, and the twofold scaled PID were recorded for 2000 repetitions of the basic time interval $T = 51.2$ ms. Thus $N_{50} \equiv N_{51.2 \text{ ms}} = 2000$, whereas $N_{200} \equiv N_{204.8 \text{ ms}} = 500$. This required approximately 100 s for each of the three sets of data. The PST histogram has no meaning for spontaneous activity. (ii) For pure tones, the PNDs were constructed from 1000 repetitions of the counting time interval T ($N_{50} = 1000$ and $N_{200} = 250$). Data were obtained for various stimulus frequencies and levels. Three pure-tone frequencies were used. The first was at the CF, and the other two were below and above the CF. All the frequencies were automatically selected from the FTC. The CF was chosen at the point of maximum sensitivity, and the other two frequencies were chosen at points on the FTC where the sensitivity was 15 dB below its maximum value. At each frequency, the measurements commenced at a SPL of -20 dB *re*: FTC threshold at that frequency. They were repeated at 10-dB increments up to a maximum of $+70$ dB *re*: FTC threshold. PST histograms were simultaneously recorded. (iii) For

broadband Gaussian noise stimuli, the PNDs were also obtained from 1000 repetitions of the counting time ($N_{50} = 1000$ and $N_{200} = 250$). The lowest rms level of the noise was about -50 dB *re*: threshold. A set of data was obtained for each 10-dB increment in the noise level, up to a level of about $+30$ dB *re*: threshold. In fact, the maximum level used in each of the above experiments was restricted by the drive limitations of the acoustic transducer, and the desire to avoid acoustic trauma. The voltage applied from the signal source was never more than 3.0 V (peak). For tonal stimuli this corresponded to a maximum of 90 dB SPL. For noise stimuli the maximum SPL level was much lower.

The collection of a full set of data for a single frequency, over the range of allowed stimulus levels, required about 7 min. The total data collection time for the three frequencies plus noise plus spontaneous events was approximately 33 min. Thus complete sets of data were collected only on selected units. In the data we report, the spike signal-to-noise ratio was high throughout the course of the experiment. FTCs were often collected both before and after data collection to verify the stability of the unit and to be sure that we were not observing injury discharge. Furthermore, it was possible to record from some units for more than 1½ h so that the same set of measurements could be repeated. In these cases, the results compared well, indicating that our measurements were stable and reproducible. PND experiments were performed with ten cats. In order to eliminate interanimal variability, we initially intended to present data from a single cat. However, the relatively long holding time requirement limited the number of units that we could study in a single experiment. The data that we present is therefore drawn from two cats. The PST data and the long-time PND data will be presented in future work, as indicated earlier.

II. RESULTS

Results are presented in the form of PNDs and various statistics of the PND, namely the count mean $\bar{n}(T)$, count variance $\sigma^2(T)$, and count mean-to-variance ratio $R(T)$. The data that we display are drawn from a number of units studied during two experiments carried out on 17–18 February 1982 and on 5–6 May 1982. FTCs for the eight units discussed in detail are presented in Fig. 3. They can be identified by the number marked underneath each FTC.

Liberman (1978) has classified auditory units on the basis of their spontaneous rate. We use the following three groupings: (i) high spontaneous (>18 spikes/s), (ii) medium spontaneous (0.5–18 spikes/s), and (iii) low spontaneous (<0.5 spikes/s). A second selection criterion that may be useful is the CF of the unit; we classify units with CFs <5.0 kHz as low-frequency units, and those with CFs >5.0 kHz as high-frequency units.

In Figs. 4–9 we present PND measurements conducted on units with high-, medium-, and low-spontaneous rates, with CFs at low and high frequencies. Our data are further broken down into units that do and do not display obvious spike pairs. The object of these divisions is to explore possible relationships between PND behavior and the physiological characteristics of particular units. Explanations of the PNDs are provided in the figure captions.

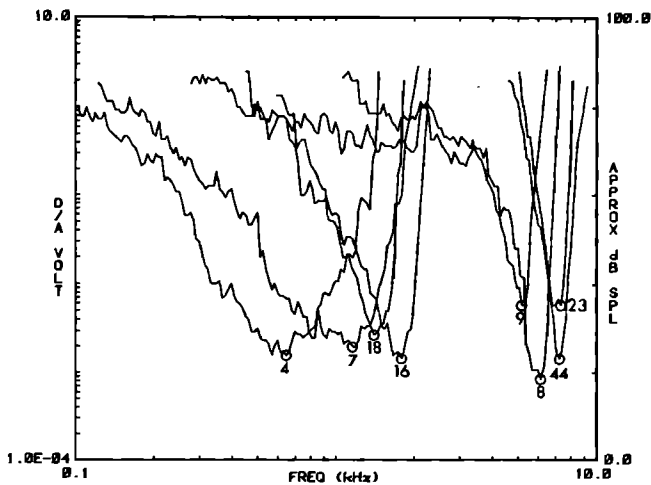


FIG. 3. Neural-threshold rate frequency tuning curves (FTCs) for the eight units reported in this study. The FTC was computed in accordance with an algorithm reported by Kiang *et al.* (1970), and by Liberman (1978). The use of this algorithm in our system has been discussed by Allen (1983). The left ordinate is calibrated in voltage applied to the acoustic driver whereas the right ordinate is calibrated in approximate dB SPL. A unit number is associated with each curve. Circles show the characteristic frequencies (CFs).

A. Count mean, variance, and mean-to-variance ratio

A number of statistics of the PNDs provide useful information in compact form. In the following, we examine the

count mean (dotted curve, denoted M), count variance (dashed curve, denoted V), and count mean-to-variance ratio (solid curve, denoted R) calculated from the ordinary PNDs. In the right-most column of Figs. 4–7, the abscissa represents the dB level of the stimulus *re*: FTC. The point marked S represents no external stimulus (spontaneous counts) and the tick marks represent 10-dB increments. In Figs. 4 and 5, the upper three panels in the right-most column correspond to the three pure-tone stimuli (below, at, and above CF, respectively). The bottom right-most panel represents the results for noise. In Figs. 6 and 7, the results are all for pure-tone stimuli at CF. As previously stated, the equivalent noise stimulus levels are about 30 dB below the pure-tone levels.

1. High-spontaneous units

a. Low CF. In Fig. 4 the data are presented for unit no. 4 (17 February 1982) which is a *high-spontaneous, low-frequency* unit. The PNDs for unit no. 4 are also shown. The count mean $M \equiv \bar{n}(T)$ represents the average number of spikes registered in the time interval T . It is proportional to the rate function of the unit (Abbas and Sachs, 1976; Javel *et al.*, 1978). In this (high spontaneous) unit, M shows only a modest increase as the stimulus level is raised (for all stimuli shown). The count variance $V \equiv \sigma^2(T)$ is lower than M in

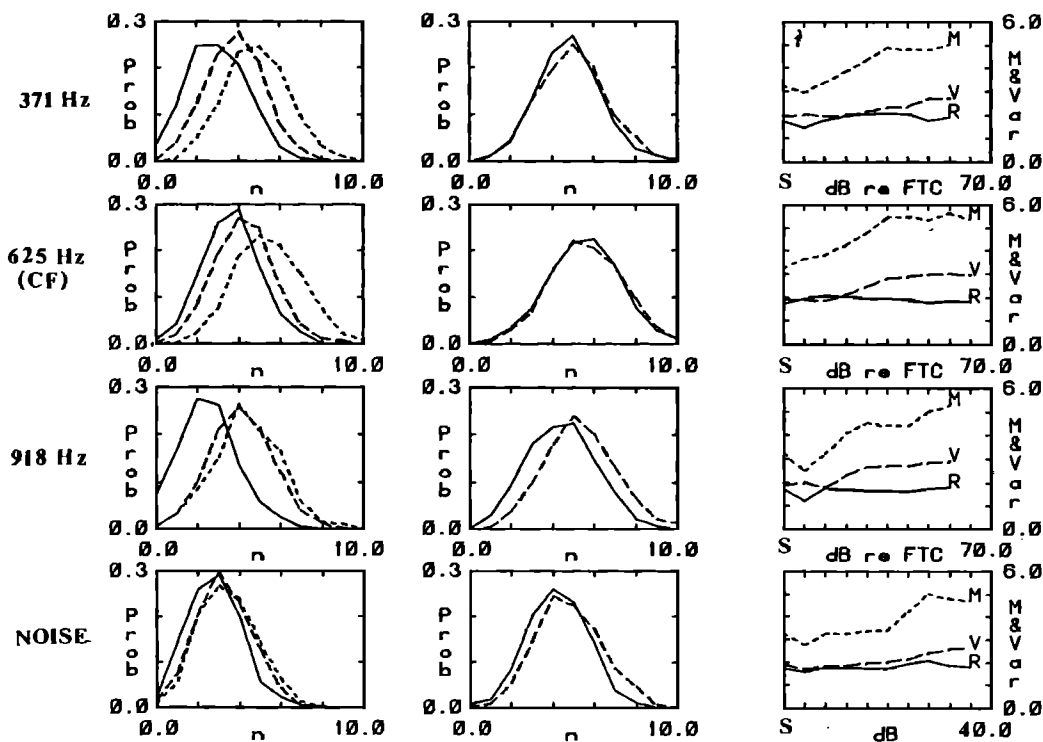


FIG. 4. Pulse-number distributions (PNDs) for a *high-spontaneous* (63.9 counts/s), *low-frequency* (CF = 625 Hz) unit (no. 4, 17 February 1982) with a threshold of about 23 dB SPL (the FTC is shown in Fig. 3). Data are presented for pure-tone stimuli at three different frequencies, and for noise. Data in rows 1–3 correspond to stimulus frequencies $f_T = 371$ Hz (below CF), $f_T = 625$ Hz (at CF), and $f_T = 918$ Hz (above CF). Data in row 4 are for broadband periodically reproduced Gaussian noise, with period $T = 51.2$ ms (this corresponds to a single payout of the D/A converter driving the sound delivery system and is also the counting time). In column 1, we present PNDs for low stimulus levels (solid, dashed, and dotted curves represent -20 , 0 , and 20 dB *re*: FTC, respectively), and in column 2 for high stimulus levels (solid and dashed curves represent 30 and 50 dB, respectively). The sound pressure is specified in dB relative to the FTC SPL at each frequency. To convert these relative values into absolute values (*re*: 0.0002 dyn/cm²), we must add the SPL at the FTC threshold to these numbers. Therefore, for this unit, absolute SPL $\approx 23 +$ dB (*re*: FTC). For broadband noise (row 4) the SPL cannot be related to the FTC values in a simple way. Roughly, the lowest level for noise is about -50 dB *re*: the CF FTC value, and the increments remain 20 dB. Plots of the PND count mean (dotted curve, denoted M), count variance (dashed curve, denoted V), and mean-to-variance ratio (solid curve, denoted R), versus dB level, are presented in column 3. S represents no external stimulus (spontaneous counts). The next tick mark to the right is -20 dB *re*: FTC; each successive tick mark is a 10-dB increase in the stimulus level. Each PND shown here consists of 1000 samples, with $T = 51.2$ ms.

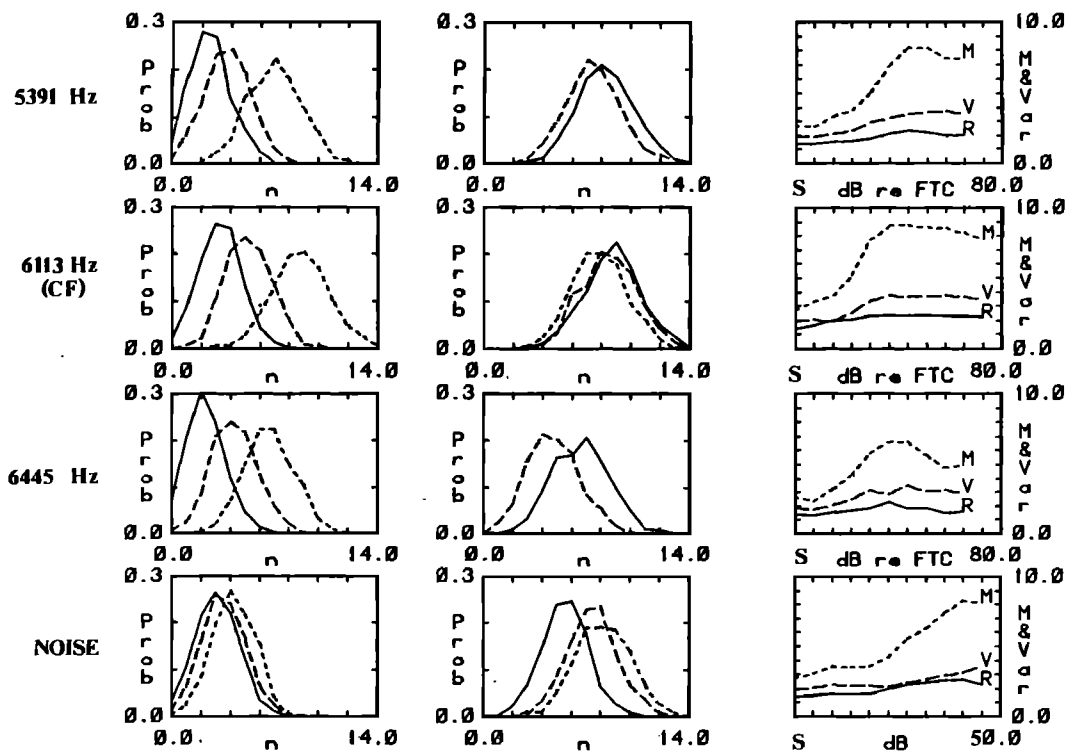


FIG. 5. PNDs and PND statistics for a *high-spontaneous* (53.7 counts/s), *high-frequency* (CF = 6113 Hz) unit (no. 8, 5 May 1982) with a threshold of about 20 dB SPL (the FTC is shown in Fig. 3). Data in rows 1–3 correspond to $f_T = 5391$ Hz (below CF), $f_T = 6113$ Hz (at CF), and $f_T = 6445$ Hz (above CF). Data in row 4 correspond to noise. In column 1, solid, dashed, and dotted curves represent $-20, 0,$ and 20 dB *re: FTC*, respectively. In column 2 they are $30, 50,$ and 70 dB *re: FTC*, respectively. Each PND consists of 1000 samples, with $T = 51.2$ ms. Note that in column 2 for pure-tone stimuli, the solid curves stand to the right of the dashed curves. This reflects a decreasing rate with increasing stimulus level, as evidenced by M in column 3. Such behavior has been observed by many investigators (e.g., see Kiang *et al.*, 1969; Kiang and Moxon, 1972; McGee *et al.*, 1981).

magnitude, but is seen to follow the same general trend as the mean. This is apparent from the behavior of $R \equiv R(T)$, which turns out to be remarkably independent of stimulus level for all four different stimuli. In this case (as is usual) $R > 1$; the process is more regular than the Poisson, and is therefore referred to as sub-Poisson or underdispersed. It is clear from the Fig. 4 that $1 \leq R \leq 2$, which is the usual range adopted by this parameter for most (but not all) units.

b. High CF. The behavior of $M, V,$ and R for unit no. 8 (5 May 1982), which is a *high-spontaneous, high-frequency* unit is shown in Fig. 5. The PNDs for unit no. 8 are also shown. Although the firing rate shows a more dramatic increase than that illustrated in Fig. 4, the value of R for this unit is also substantially independent of stimulus level for all the stimuli. A slight increase of R may be discerned from the lowest to the highest levels of the stimulus. Again, $R \sim 2$.

2. Medium-spontaneous units

a. Low CF. Similarly, $M, V,$ and R for unit no. 16 (5 May 1982), which is a *medium-spontaneous, low-frequency* unit driven at CF, are shown in the right panel of Fig. 6(a). The PNDs for unit no. 16 are also shown. Again, the data provide $1 \leq R \leq 2$.

b. High CF. $M, V,$ and R for unit no. 9 (5 May 1982), which is a *medium-spontaneous, high-frequency* unit driven

at CF, are presented in the right panel of Fig. 6(b). The PNDs for unit no. 9 are also shown. The firing rates both show a

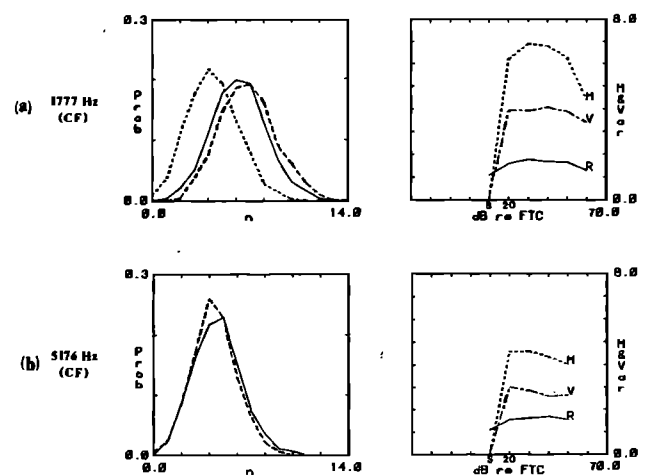


FIG. 6. (a) PNDs and PND statistics for a *medium-spontaneous* (1.95 counts/s), *low-frequency* (CF = 1777 Hz) unit (no. 16, 5 May 1982) with a threshold of about 23 dB SPL (the FTC is shown in Fig. 3). (b) PNDs and PND statistics for a *medium-spontaneous* (1.95 counts/s), *high-frequency* (CF = 5176 Hz) unit (no. 9, 5 May 1982) with a threshold of about 36 dB SPL (the FTC is shown in Fig. 3). The following apply to both (a) and (b): the PNDs (column 1) and the count mean, variance, and mean-to-variance ratio (column 2) are collected at the CF. The solid, dashed, and dotted PND curves represent $+20, 40,$ and 60 dB *re: FTC*, respectively. Each PND consists of 1000 samples, with $T = 51.2$ ms.

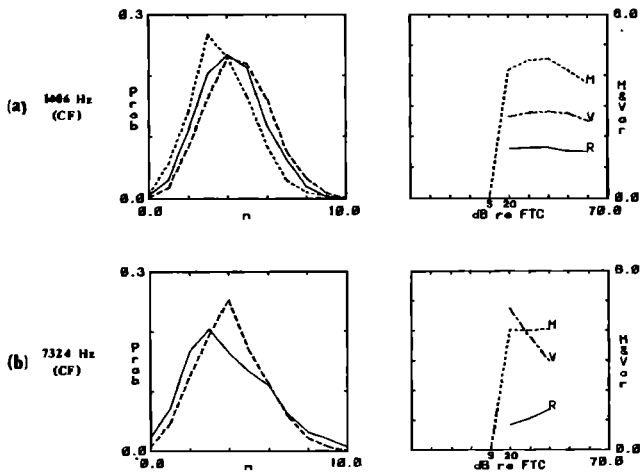


FIG. 7. (a) PNDs and PND statistics for a *low-spontaneous* (0 counts/s), *low-frequency* (CF = 1406 Hz) unit (no. 18, 5 May 1982) with a threshold of about 30 dB SPL (the FTC is shown in Fig. 3). (b) PNDs and PND statistics for a *low-spontaneous* (0 counts/s), *high-frequency* (CF = 7324 Hz) unit (no. 23, 5 May 1982) with a threshold of about 37 dB SPL (the FTC is shown in Fig. 3). The following apply to both (a) and (b): The PNDs (column 1) and the count mean, variance, and mean-to-variance ratio (column 2) are collected at the CF. The solid, dashed, and dotted PND curves represent +20, 40, and 60 dB *re*: FTC, respectively. Each PND consists of 1000 samples, with $T = 51.2$ ms.

decrease above 30 dB *re*: FTC. Nevertheless, the values for R are again quite constant, such that $1 \lesssim R \lesssim 2$ even under conditions of spontaneous firing.

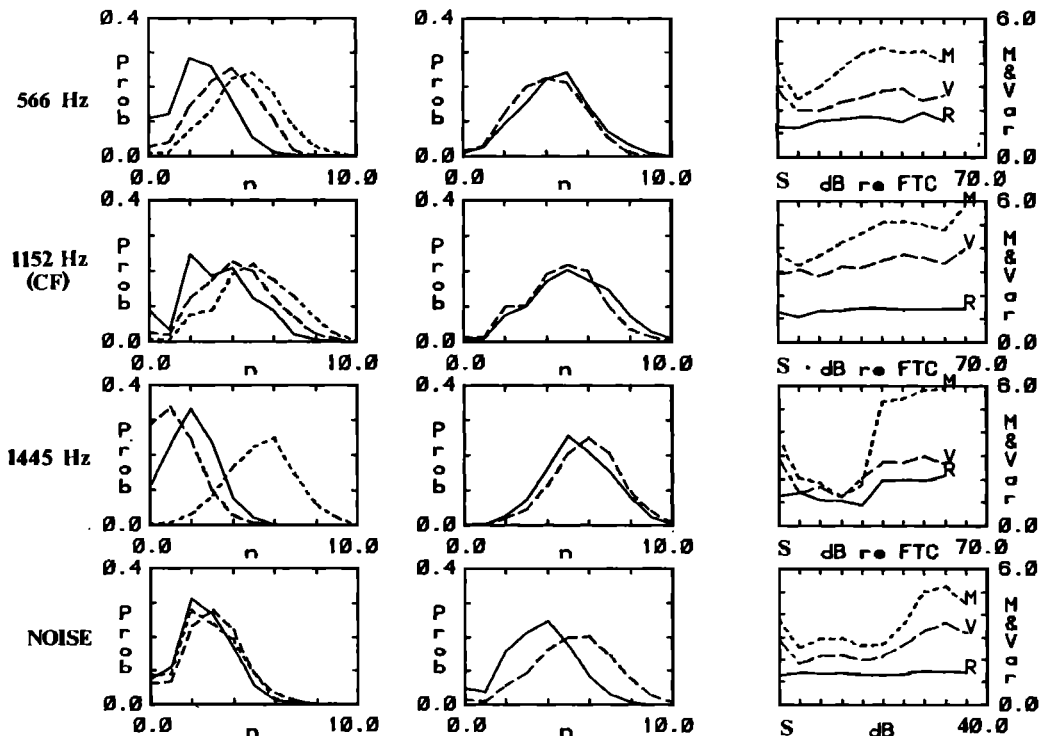


FIG. 8. PNDs and PND statistics for a *high-spontaneous* (74.2 counts/s), *low-frequency* (CF = 1152 Hz) unit (no. 7, 17 February 1982) with a threshold of about 26 dB SPL (the FTC is shown in Fig. 3). Data in rows 1–3 correspond to $f_T = 566$ Hz (below CF), $f_T = 1152$ Hz (at CF), and $f_T = 1445$ Hz (above CF). Data in row 4 correspond to noise. In column 1, solid, dashed, and dotted curves represent -20 , 0 , and 20 dB *re*: FTC, respectively. In column 2 the solid and dashed curves are 30 and 50 dB *re*: FTC, respectively. Each PND consists of 1000 samples, with $T = 51.2$ ms. The PNDs appear quite different from those shown for unit 4 in Fig. 4 (which is also a high-spontaneous, low-frequency unit with a similar FTC), and Figs. 5–7. In particular, these PNDs have a more jagged appearance, particularly at the CF. Closer inspection reveals that this scalloping results from an enhanced likelihood of occurrence of even numbers of neural spikes n over odd numbers of spikes. This reflects the presence of spike pairs within the counting time T . Although it is not always the case, for this particular unit the pulse pairs are also clearly evident in the (spontaneous) PID, as will be discussed subsequently (see Fig. 12).

3. Low-spontaneous units

a. Low CF. The right panel of Fig. 7(a) shows the behavior of M , V , and R for unit no. 18 (5 May 1982), which is a *low-spontaneous, low-frequency* unit driven at CF. The PNDs for unit no. 18 are also shown.

b. High CF. Figure 7(b) shows M , V , and R for unit no. 23 (5 May 1982), which is a *low-spontaneous, high-frequency* unit driven at CF. The PNDs for unit no. 23 are also shown. The firing rates of these units do not change appreciably in the stimulus range investigated; the values for the mean-to-variance ratio R fall within the range $1 \lesssim R \lesssim 2$. The values of V and R carry no meaning at zero stimulus (S) since no spontaneous counts were recorded for these zero-spontaneous units.

B. Count mean, variance, and mean-to-variance ratio for units that display spike pairs

1. High-spontaneous unit, low CF

The quantities M , V , and R for unit no. 7 (17 February 1982) are displayed in Fig. 8. This is a *high-spontaneous, low-frequency* unit that generates spike pairs. The PNDs for unit no. 7 are also shown. The growth of the firing rate is rather modest for this unit; indeed it is similar to that shown in Fig. 4 (a high-spontaneous, low-frequency unit that does not generate obvious spike pairs). The value of R does not vary sub-

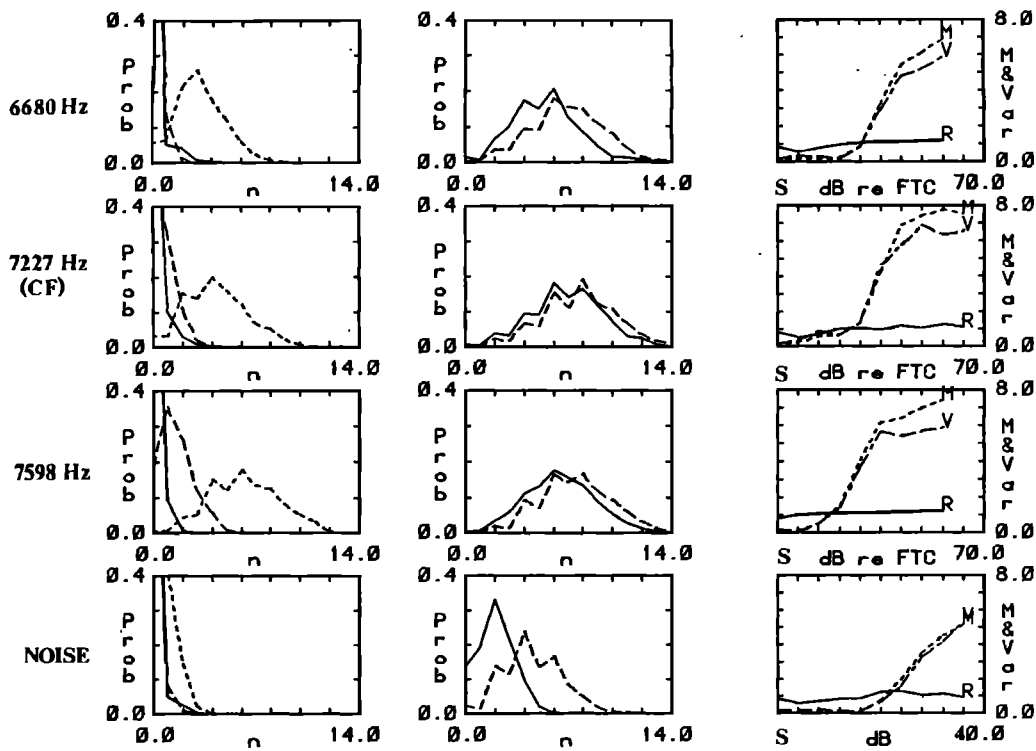


FIG. 9. PNDs and PND statistics for a *medium-spontaneous* (4.1 counts/s), *high-frequency* (CF = 7227 Hz) unit (no. 44, 17 February 1982) with a threshold of about 23 dB SPL (the FTC is shown in Fig. 3). Data in rows 1–3 correspond to $f_T = 6680$ Hz (below CF), $f_T = 7227$ Hz (at CF), and $f_T = 7598$ Hz (above CF). Data in row 4 correspond to noise. In column 1, solid, dashed, and dotted curves represent -20 , 0 , and 20 dB re: FTC, respectively. In column 2 the solid and dashed curves are 30 and 50 dB re: FTC, respectively. Each PND consists of 1000 samples, with $T = 51.2$ ms. The data are quite different from those shown in Fig. 6(b) (which also represent a *medium-spontaneous, high-frequency* unit), and Figs. 4, 5, 6(a), and 7. Rather, they display the clear scalloping that is also evident in Fig. 8, a unit with quite different spontaneous-rate and frequency-response characteristics. Again, the scalloping reflects the presence of spike pairs within the counting time T ; in this case it is noticeable for stimuli at all frequencies as well as for noise.

stantially for this unit, and again falls within the range $1 \leq R \leq 2$ for all the stimuli. We have observed, however, that units generating obvious spike pairs tend to fall toward the lower end of this range. This is probably a consequence of the additional variance imparted to the counting process by the spike-pair occurrences.

2. Medium-spontaneous unit, high CF

The results for M , V , and R for unit no. 44 (17 February 1982) are presented in Fig. 9. This is a *medium-spontaneous, high-frequency* unit that generates spike pairs. The PNDs for unit no. 44 are also shown. The growth of the firing rate is substantial, as is evident from Fig. 9. R is seen to hover about unity for this spike-pair generating unit, for all four different stimuli.

C. Spontaneous PNDs and PIDs

1. High-spontaneous unit, low CF

Also of interest is the statistical nature of the spontaneous (undriven) neural activity in the primary auditory fibers; in particular, it is of interest to compare this with the stimulus-evoked activity. The spontaneous PND for unit no. 4 (17 February 1982) is presented in Fig. 10(a). This is a *high-spontaneous, low-frequency* unit. The driven PNDs and PND statistics are shown in Fig. 4. The shape of the spontaneous PND resembles those of the driven PNDs. The mean-to-

variance ratio $R = 1.72$, representing underdispersion relative to the Poisson distribution.

In Fig. 10(b) we show the pulse-interval distribution (PID) for unit no. 4. This PID is the usual unscaled version $P^{(1)}(t)$, representing the distribution of the time intervals between adjacent events [see Fig. 1(c)]. To reduce noise, the data in four adjacent time bins have been averaged. Thus the bin width for all PIDs shown is $100 \mu\text{s}$. The phase-locking behavior evident in Fig. 10(b) may be caused by low-frequency noise leaking into the chamber. At these low frequencies the isolation provided by our double-walled chamber may not be sufficient to prevent some of this noise from leaking through to the animal. Also, any local noise such as a breathing artifact, will produce such peaks in a sensitive unit. [This may also affect the PND shown in Fig. 10(a).] The mean time interval $\bar{t}^{(1)} = 10.4$ ms [but $T/\bar{n}(T) = 15.7$ ms $> \bar{t}^{(1)}$, as expected from the truncation of $P^{(1)}(t)$ —see Sec. I B]. The standard deviation of the interval distribution is $\sigma_t = 8.8$ ms. This provides a coefficient of variation $CV^{(1)} = \sigma_t/\bar{t}^{(1)} \approx 0.85$, also representing underdispersion relative to the Poisson process. Note that the mode (most probable time interval) is about 1.3 ms. Note also that the envelope of the PID does not resemble a decaying exponential.

An expanded view of the initial portion of the PID is shown in Fig. 10(c). Note the complete absence of events for $t < 1.0$ ms; part of this (≈ 0.95 ms) represents deliberate instrumental dead time. Also observe the rather sharp initial

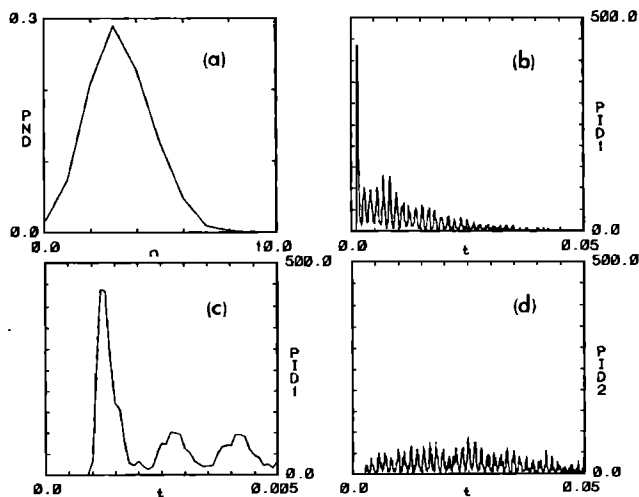


FIG. 10. (a) Spontaneous PND for unit no. 4 (17 February 1982), which is a *high-spontaneous, low-frequency* unit. The FTC is shown in Fig. 3, and the driven PNDs and PND statistics are displayed in Fig. 4. The shape of the spontaneous PND resembles those of the driven PNDs. The number of samples is 2000 and $T = 51.2$ ms. (b) Pulse-interval distribution (PID) for unit no. 4. This PID is the usual unscaled version $P^{(1)}(t)$, representing the distribution of the time intervals between adjacent events [see Fig. 1(c)]. The number of samples is 2000. The phase-locking behavior evident above is probably due to low-frequency noise leaking into the chamber and to local noise. (c) Expanded view of the beginning portion of the PID shown in (b). Note the complete absence of events for $t < 1.0$ ms, representing deliberate instrumental dead time. Also observe the rather sharp initial peak in the PID; its width is only about 0.4 ms. This represents the occurrence of neural spike pairs with a separation of 1.3 ± 0.2 ms. (d) Second-order pulse-interval distribution $P^{(2)}(t)$, representing the distribution of the time intervals between *every other* event. The number of samples is again 2000. The phase locking is evident [as it is also from $P^{(1)}(t)$].

peak in the PID; its width is only about 0.4 ms. This indicates the occurrence of neural spike pairs with a fixed separation of 1.3 ± 0.2 ms (it is possible that some closer spike pairs also occur but are obfuscated by the instrumental dead time). Although closely spaced pairs of spikes are evidenced in the PID in this case, the PND shown in Fig. 10(a) does not display the scalloping that might be expected as a result of these spike pairs. Closer inspection reveals that an enhancement of even count numbers does occur, however.

For comparison, the second-order (scaled) pulse-interval distribution $P^{(2)}(t)$, representing the distribution of the time intervals between *every other* event, is displayed in Fig. 10(d). The absence of a sharp peak at short time intervals means that alternate events are not closely spaced. This provides evidence that the spike pairs revealed in Fig. 10(b) and (c) occur as adjacent events. The distribution $P^{(2)}(t)$ is a special case of the joint pulse-interval distribution considered by Gerstein and Kiang (1960). It turns out that the mean time interval $\bar{t}^{(2)} = 23.9$ ms, the standard deviation $\sigma_t^{(2)} = 11.8$ ms, and $CV^{(2)} = 0.49$. Phase locking is evident [as it is also from $P^{(1)}(t)$].

2. High-spontaneous unit, high CF

We next consider [in Fig. 11(a)], the spontaneous PND for a *high-spontaneous, high-frequency* unit [unit no. 8 (5 May 1982)]. The driven PNDs and PND statistics are shown

in Fig. 5. The shape of the spontaneous PND resembles those of the driven PNDs. Here, $R = 1.42$ representing underdispersion relative to the Poisson distribution. In Fig. 11(b) we present $P^{(1)}(t)$ for unit no. 8. The beginning portion of $P^{(1)}(t)$ is expanded in Fig. 11(c). Again, the instrumental dead-time period is just under 1 ms. There is an initial peak in the PID representing spike pairs separated by 1.0 ± 0.1 ms, yet the PND shown in Fig. 11(a) does not display scalloping. The measured statistics for $P^{(1)}(t)$ are $\bar{t}^{(1)} = 13.7$ ms [but $T/\bar{n}(T) = 18.6$ ms $>$ $\bar{t}^{(1)}$], $\sigma_t^{(1)} = 9.6$ ms, and $CV^{(1)} = 0.70$, also representing underdispersion. Phase locking is not evident for this high-frequency unit. In Fig. 11(d), we display $P^{(2)}(t)$, with $\bar{t}^{(2)} = 24.6$ ms, $\sigma_t^{(2)} = 10.9$ ms, and $CV^{(2)} = 0.44$. Evidence for phase locking is again absent.

3. High-spontaneous spike-pair producing unit, low CF

The spontaneous PND for unit no. 7 (17 February 1982) is displayed in Fig. 12(a). This is a *high-spontaneous, low-frequency* unit. The driven PNDs and PND statistics are shown in Fig. 8. The shape of the spontaneous PND resembles those of the driven PNDs. The presence of scalloping (indicating spike pairs) is evident, and $R = 1.30$, which indicates underdispersion relative to the Poisson distribution. In Fig. 12(b), we show $P^{(1)}(t)$ for unit no. 7. The statistics are $\bar{t}^{(1)} = 7.4$ ms [but $T/\bar{n}(T) = 13.5$ ms $>$ $\bar{t}^{(1)}$], $\sigma_t^{(1)} = 9.3$ ms, and $CV^{(1)} = 1.25$, indicating overdispersion. The apparent discrepancy with the underdispersion evidenced by the PND may be because large t are excluded due to the 50-ms maximum time interval that our histogram hardware can register. It may also result from the fact that the PND and PID are different measures. The most prominent feature in the PID is a large spike of probability for small intervals (the mode is 1.05 ms), although phase locking is also evident on

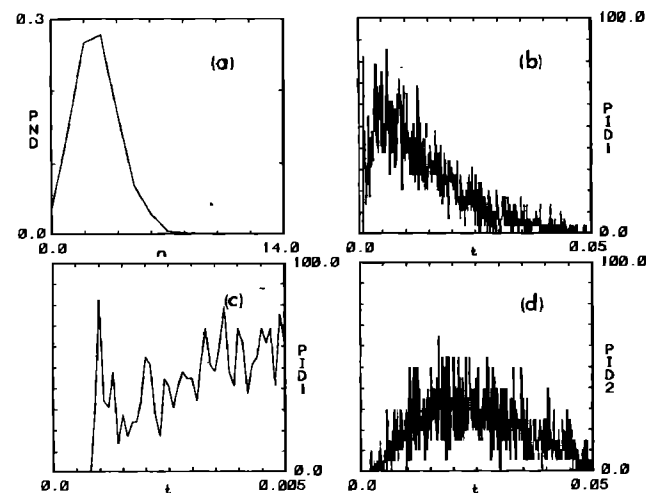


FIG. 11. (a) Spontaneous PND for unit no. 8 (5 May 1982), which is a *high-spontaneous, high-frequency* unit. The FTC is shown in Fig. 3, and the driven PNDs and PND statistics are shown in Fig. 5. The shape of the spontaneous PND resembles those of the driven PNDs. The number of samples is 2000, and $T = 51.2$ ms. (b) Pulse-interval distribution $P^{(1)}(t)$ for unit no. 8. The number of samples is 2000. Phase locking is not evident for this high-frequency unit. (c) Expanded view of the beginning portion of $P^{(1)}(t)$. Again, the instrumental dead-time period is about 1 ms; there is an initial peak in the PID representing spike pairs separated by 1.0 ± 0.1 ms. (d) $P^{(2)}(t)$. The number of samples is again 2000. Evidence for phase locking is absent.

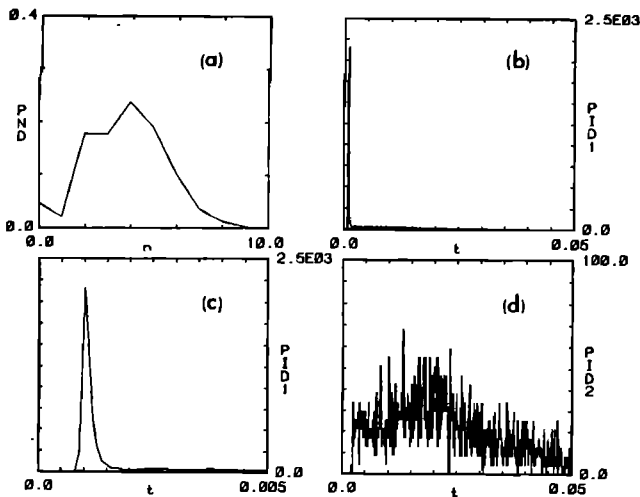


FIG. 12. (a) Spontaneous PND for unit no. 7 (17 February 1982), which is a *high-spontaneous, low-frequency* unit. The FTC is shown in Fig. 3; the driven PNDs and PND statistics are shown in Fig. 8. The shape of the spontaneous PND resembles those of the driven PNDs (there was, however, some unavoidable low-frequency noise leaking into the chamber). The presence of scalloping (indicating pulse pairs) is evident. The number of samples is 2000 and $T = 51.2$ ms. (b) Pulse-interval distribution $P^{(1)}(t)$ for unit no. 7. The number of samples is 2000. The most prominent feature in the PID is a large spike of probability for small intervals, although phase locking is also evident on an expanded scale (not shown). This distribution has many features in common with the one displayed in Fig. 10(b). (c) Expanded view of the beginning portion of $P^{(1)}(t)$. The instrumental dead time is about 1 ms. The initial peak in the PID represents adjacent spike pairs separated by 1.05 ± 0.1 ms. The pairs are sufficiently prominent in this case to be clearly seen as scalloping in the PND displayed in (a). (d) $P^{(2)}(t)$. The number of samples is again 2000. Evidence for phase locking is not easily discerned.

an expanded scale (not shown). This distribution has many features in common with the one displayed in Fig. 10(b). An expanded view of the beginning portion of $P^{(1)}(t)$ is shown in Fig. 12(c). The instrumental dead time is about 0.95 ms. The initial peak in the PID represents adjacent spike pairs separated by 1.05 ± 0.1 ms. The pairs are sufficiently prominent in this case to be clearly seen as scalloping in the PND displayed in Fig. 12(a). In Fig. 12(d), we present $P^{(2)}(t)$, with $\bar{t}^{(2)} = 22.1$ ms, $\sigma_t^{(2)} = 11.9$ ms, and $CV^{(2)} = 0.54$. Evidence for phase locking is not easily discerned. The absence of a sharp peak at short time intervals provides evidence that the pulse pairs discussed in connection with Fig. 12(a)–(c) occur as adjacent events.

4. Medium-spontaneous spike-pair producing unit, high CF

In Fig. 13(a) we present the spontaneous PND for unit no. 44 (17 February 1982), which is a *medium-spontaneous, high-frequency* unit. The driven PNDs and PND statistics are shown in Fig. 9. The shape of the spontaneous PND resembles those of the driven PNDs, and R is quite low at 0.82. Although not immediately evident visually because of the low mean, strong scalloping is present. Figure 13(b) shows $P^{(1)}(t)$ for unit no. 44. The statistics are not meaningful since data could be collected only up to $t = 50$ ms, which is insufficient for a unit with this low a spontaneous rate. This demonstrates the well-known difficulty of collecting useful pulse-interval data for medium- and low-spontaneous units. Statistically significant PND data may be obtained for these units, however, as is clear from Eq. (6), which shows that

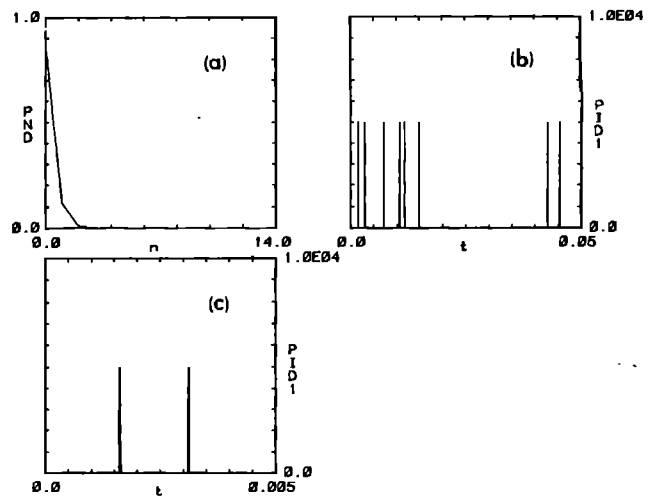


FIG. 13. (a) Spontaneous PND for unit no. 44 (17 February 1982), which is a *medium-spontaneous, high-frequency* unit. The FTC is shown in Fig. 3; the driven PNDs and PND statistics are shown in Fig. 9. The shape of the spontaneous PND resembles those of the driven PNDs. Although not visually evident because of the low mean, strong scalloping is present. The number of samples is 2000, and $T = 51.2$ ms. (b) Pulse-interval distribution [$P^{(1)}(t)$] for unit no. 4. The number of samples is 2000. The statistics are not meaningful since data could be collected only up to $t = 50$ ms, which is insufficient for a unit of this low a spontaneous rate. (c) Expanded view of the beginning portion of $P^{(1)}(t)$. The smallest interspike interval occurred at about 1.6 ms, which is longer than the expected absolute refractory period. Data for $P^{(2)}(t)$ could not be collected because of an insufficient spontaneous rate.

$\Delta R(T)$ is approximately independent of $\bar{n}(T)$. An expanded view of the beginning portion of $P^{(1)}(t)$ is shown in Fig. 13(c). All that can be said is that the smallest interspike interval occurred at about 1.6 ms, which is longer than the expected absolute refractory period. Data for $P^{(2)}(t)$ could not be collected because of an insufficient spontaneous rate.

III. DISCUSSION

The PND provides the experimenter with a useful window on the coding of information in the neural spike train. For a counting time that is sufficiently long it permits the observation of clusters of spikes, in which the times of occurrence of individual spikes may be random. Spike pairs are a special case of clusters. For clusters to appear in the PST histogram, their occurrences must be synchronized with the stimulus, and the intervals between the events must be fixed. Similarly, a spike cluster will appear in the PID only when the intervals between the events are fixed. The PND, on the other hand, will reflect the presence of such clusters even when their occurrences are not synchronized with the stimulus and/or the time intervals are variable, as long as the counting time is sufficiently large.

The PND also succinctly displays regularity in a point process. This is most apparent in two limiting examples: (i) the Poisson PND which, as is well known, reflects zero-memory behavior; and (ii) the PND for a periodic pulse train which reflects long-term memory. (The initial phase of the periodic pulse train is taken to be uniformly distributed to preserve stationarity—see Teich *et al.*, 1984, for a discussion of this subtlety.)

There are also different, practical reasons for using the

PND to compile neural data: (i) time jitter and time quantization in the measurement system become unimportant so that PND data are not contaminated by these instrumental effects [we have already pointed out that the PID and PST can suffer from such limitations, as shown by Johnson (1978)], and (ii) it provides a statistically valid measure for studying units that fire at low rates; under these conditions it is difficult to collect a statistically significant PID or PST.

The behavior of the PND is most readily captured by its mean count $\bar{n}(T)$ and mean-to-variance ratio $R(T)$, which are equivalent to the first two moments of the counting distribution. Of course, the mean count is directly proportional to the usual rate function for the unit. The form and magnitude of $R(T)$ provide measures for the nature and regularity of the underlying spike train. If events are generally well organized along the time axis, the count variance will be small (since the number of events in T will be relatively constant) and $R(T)$ will be large. On the other hand, if random spike clusters or pairs appear, the variance will be large (due to the fact that sometimes the clusters will be captured in T and sometimes they will not) and $R(T)$ will then be small. For the zero-memory Poisson counting distribution, $R(T) = 1$ for all T , whereas for the highly regular pulse train, $R(T) \rightarrow \infty$ for sufficiently large T (Teich *et al.*, 1984).

A. Role of various neurophysiological effects on the PND and on $R(T)$

Refractoriness (absolute and/or relative) introduces memory into the spike occurrences, thereby increasing the regularity of the spike train (the occurrence of a spike makes it less likely that a subsequent spike will occur close to it in time). As a particular example, it converts a HPP into a renewal point process (RPP). Because of the enhanced regularity, refractoriness drives $R(T)$ above unity (Cox, 1962) for T large enough such that the regular spacings are captured. Expressions for $\bar{n}(T)$, $R(T)$, and $p(n, T)$ for the nonparalyzable dead-time-modified HPP (which we refer to as the DTMPP) are well known (Ricciardi and Esposito, 1966; Müller, 1974; Cantor and Teich, 1975). $R(T)$ may be simply expressed in terms of $\bar{n}(T)$ as

$$R(T) \simeq (1 - \bar{n}\tau_d/T)^{-2}, \quad (10)$$

where $\bar{n} \equiv \bar{n}(T)$ is the observed mean count, τ_d is the dead time, and T is the counting time. The term nonparalyzable indicates that hypothetical events that would have occurred during the dead-time period are ignored and, furthermore, do not extend it (i.e., do not paralyze the counter). Dead time causes an increase in $R(T)$ even when the initial process differs from Poisson (Prucnal and Teich, 1983).

Phase locking or synchrony (Johnson, 1980) also introduces memory into the process, since spike occurrences are separated from each other by the cycles of the stimulus. Thus synchrony increases the regularity of the events and thereby also drives up $R(T)$. The count mean-to-variance ratio thus provides a measure for the existence of synchrony that differs from the usual synchronization index (SI). The latter is more specific to the occurrence of synchrony *per se* since $R(T)$ is also affected by other factors such as refractoriness

and spike clusters. Nevertheless, $R(T)$ may be a useful parameter for special purposes, such as investigating the existence of synchrony in high-CF cochlear nerve fibers where instrumental effects may compromise the SI as an unbiased measure. In the simplest models for synchrony, at most a single spike may occur on any cycle of the stimulus and each spike is generated in accordance with an independent Bernoulli trial. In this case, $p(n, T)$ will be the simple binomial distribution for T sufficiently large. The quantities $\bar{n}(T)$ and $R(T)$ are, of course, well known for the binomial. $R(T)$ is expressed in terms of $\bar{n}(T)$ as

$$R(T) \simeq (1 - \bar{n}/M)^{-1}, \quad (11)$$

where again \bar{n} is the observed mean count and M is the number of trials (cycles) presenting themselves for Bernoulli transmission in the time T .

Actually, synchrony and refractoriness need not be separable in the simple way described above. An alternative model would have the synchronization generate an inhomogeneous Poisson process (Siebert, 1968) that is then modified by refractoriness. Analytical results are available for $\bar{n}(T)$ and $R(T)$ for an inhomogeneous Poisson process in the presence of nonparalyzable fixed dead time (Vannucci and Teich, 1978; Prucnal and Teich, 1983). The characteristic behavior of the mean-to-variance ratio turns out to be quite similar to that of the DTMPP. Of course, the PIDs for the two cases will differ substantially. In the absence of dead time such an inhomogeneous process leads to a Poisson PND [$R(T) = 1$] if T is large in comparison with the period of the stimulus.

The doubly stochastic Poisson process (DSPP) is yet another model sometimes used to describe auditory neural events. In this case $R(T)$ is always less than or equal to unity in the absence of dead time (Saleh, 1978). In the presence of strong dead time, however, $R(T)$ can exceed unity (Prucnal and Teich, 1983). The PID of a DSPP will not show traditional phase locking.

Finally, we examine the effect of spike clusters on the PND and on $R(T)$. Such clusters increase the variance of $p(n, T)$ and thereby decrease $R(T)$. A simple example is spike pairs. If the two constituent events of a pair occur sufficiently close in time so that they are captured in the counting time T , they will be specifically manifested as an enhancement of the probabilities of even number of events if the noise does not wash out this effect. For example, a primary HPP in which every event produces a spike pair has $R(T) = 0.5$, rather than $R(T) = 1.0$ as for the HPP itself. The existence of spike clusters causes the value of $R(T)$ to be decreased below its expected value in the absence of such clusters.

We can summarize our observations as follows. Neurophysiological effects that lead to regularized spike occurrences (e.g., refractoriness and synchrony) provide an elevation of $R(T)$, whereas neurophysiological effects associated with spike pairs or clusters provide a decrease in $R(T)$. We reiterate that such effects will be reflected in $p(n, T)$ and in $R(T)$ only if T is large in comparison with the characteristic time of the particular feature in question. Short time PND measurements cut apart both regularity and clusters, and result in a low-mean Poisson-like distribution containing little information about the underlying neural point process (Teich *et al.*, 1984).

B. Failures of conventional models in fitting PND data

It is apparent from our experiments that most units have PNDs that are more-or-less bell-shaped in nature, with $1 \leq R (T = 51.2 \text{ ms}) \leq 2$. This is true for high-, medium-, and low-spontaneous units, with low and high CFs. It is important to note that $R (T)$ is, for the most part, independent of the level and frequency of the stimulus (even when it is noise). Since $R (T)$ is generally > 1 , the underlying neural process cannot be a simple HPP or inhomogeneous Poisson process, nor can it be a DSPP without dead time.

It is widely accepted that (absolute and relative) refractoriness plays an important role in the neural point process (Kiang *et al.*, 1965; Kiang, 1984; Ricciardi and Esposito, 1966; Gray, 1967; Fienberg, 1974; Teich and McGill, 1976; Teich *et al.*, 1978; Teich and Saleh, 1981; Lütkenhöner *et al.*, 1980; Gaumond *et al.*, 1982; Johnson and Swami, 1983). It is sensible (and relatively simple) to examine the consequences of fitting the PND data by the counting distribution associated with a fixed nonparalyzable dead-time-modified Poisson point process (DTMPP). We have carried this out and the fits are for the most part quite good, yielding plausible dead-time values τ_d in the range 1–4 ms. If the underlying point process were a pure DTMPP, however, we would expect $R (T)$ to increase with \bar{n} in accordance with Eq. (10) (Teich *et al.*, 1978). The problem is that, to keep $R (T)$ as constant as it experimentally turns out to be, requires τ_d to behave as $1/\bar{n}$. This means that the dead time must decrease as the firing rate increases. We can think of no rationale for such behavior. If anything we would expect the opposite. Furthermore, the PID for the DTMPP is a shifted exponential, and does not exhibit the scalloping associated with phase locking. (The occurrence of pulse pairs is also inconsistent with this model; we will return to this point shortly.) Finally, because of pulse pairs, $R (T)$ sometimes falls below unity and this cannot be accounted for by the DTMPP.

A more complex possibility that admits $R (T) < 1$ is a Poisson process with an inhomogeneous (or stochastic) rate, modified by fixed (or relative) refractoriness. However, for all such models, $R (T)$ will exhibit a substantial dependence on the observed mean count (Teich and Diamant, 1980; Prucnal and Teich, 1983). The theoretical construct provided by Lütkenhöner *et al.* (1980) is of this form.

Another issue that makes it difficult to fit conventional models to the PND data is the existence of spike pairs. We have discerned that there is a class of units that generates spike pairs almost exclusively (for $T = 51.2 \text{ ms}$). This is apparent from the enhancement of the even values of $p(n, T)$ (see Figs. 8 and 9). This effect can occur for units of all spontaneous rates and CFs, and at all stimulus frequencies and levels. It can be shown that even a small number of added random events ($< 10\%$ of the mean) will destroy the scalloping that is visually apparent in the PND; thus units displaying such clear scalloping are generating in excess of 90% spike pairs. The experimental data show that for such units $R (T)$ also remains relatively constant, although generally at a value lower than that for units in which scalloping is not obviously present in the PND.

Many researchers have observed spike pairs in the

VIIIth-nerve process (Rupert *et al.*, 1963; Ruggero, 1973; Gaumond *et al.*, 1982; Liberman, personal communication, 1983). "Peak splitting" in the PST histogram (Johnson, 1980; Ruggero and Rich, 1983), which often appears at high stimulus levels and low frequencies, may be a manifestation of such events. From our results and from the observations of other researchers, however, spike-pair generation is not restricted to these conditions. Although spike pairs have been observed in a great many measurement paradigms (they are sometimes quite evident on the oscilloscope screen during the course of an experiment), it is clear that the PND provides a useful measure for quantifying their role. It is possible that spike pairs are present in many auditory units, but are not so discerned because of the effects of small amounts of additive noise.

Clusters of events turn out also to be present in the mammalian visual system, in recordings made at the retinal ganglion cell (optic nerve) of the cat (Barlow *et al.*, 1971). Whether these clusters are spike pairs or more random collections of spikes has not yet been ascertained, although the shot-noise-driven DSPP (SNDP) has been used as a model for Poisson pulse clusters in the visual system (Teich and Saleh, 1981; Teich *et al.*, 1982). Spike pairs have also quite often been observed in other nerve-cell discharge patterns, especially in crustaceans (see Sugano, 1983 and references therein; Holden and Winlow, 1983).

Qualitatively, the presence of such correlated spikes does not support a renewal process theory. This can be seen explicitly from the experimental PID and the twofold scaled PID (see Figs. 10–12). The RPP is not a satisfactory model, since we often find that

$$P^{(2)}(t) \neq P^{(1)}(t) * P^{(1)}(t), \quad (12)$$

where $*$ represents the convolution operation (Cox, 1962).

Finally, we can attempt to fit our data with the binomial distribution which provides the simplest model for synchrony (or synchrony/refractoriness). This leads to a mean-to-variance ratio given by Eq. (11). This distribution provides a good fit to the bell-shaped PNDs not exhibiting obvious pairs but, again, to keep $R (T)$ as constants as it turns out to be experimentally, requires the special behavior $M \simeq 1/\bar{n}$. This implies that the count rate must be inversely proportional to the stimulus frequency, which is not in accord with observation. Although this simple model fails to adequately represent the data, it does provide a useful point of departure for arriving at a more suitable model, as will be seen in Sec. III C.

C. Toward identifying the peripheral auditory neural point process and the PND

It is apparent from studies of many statistical measures (e.g., the PID, PST, and PND) that phase locking, refractoriness, and spike-cluster generation all play an important role in the primary auditory neural spike train. A mathematical model consistent with all the various measures can be constructed in terms of a cluster point process related to the Neyman–Scott type (Neyman and Scott, 1958; Saleh and Teich, 1982). One way of achieving this is to let each event of a primary process (e.g., selected zero crossings of the stimu-

lus) generate a randomly delayed cluster of secondary events. Further, let the number of events in each cluster be specified by a particular probability law (i.e., assign probabilities for zeros, singlets, pairs, triplets, etc.) and the positions by (stochastic) delay times measured from the primary event. These delay times are in part to be determined by the phase-sensitive impulse response function of the system so that a proper PID and PST result. [In the pure Neyman-Scott model, the primary process is a HPP (it is excluded from the final point process), the cluster statistics are arbitrary, and the delay times are statistically independent and identically distributed.]

The pulse-number distribution associated with such a point process will depend on the statistics of both the primary and secondary processes. For a deterministic number of selected zero crossings, and clusters consisting of only zero or one spike, the outcome is again the simple binomial. If zeros, singlets, and spike pairs are permitted, $p(n)$ turns out to be expressible as a sum of trinomials. If triplets are also permitted, the PND is a transformed sum of quadrinomials. In general, the distribution will be a transformed sum of multinomials. In the trinomial case, $R(T)$ can be either $>$ or $<$ 1, depending on the relative probabilities of the number of spikes per cluster. We have seen earlier that some units do indeed exhibit $R(T) < 1$. It is useful to note that the independence of $R(T)$ on stimulus level for the trinomial requires a special relation between the observed count rate and the number of degrees of freedom rather than the stimulus frequency as for the binomial [Eq. (11)]. The trinomial and quadrinomial results make good sense.

We repeat again that if T is not sufficiently long, the particlelike regularities and clusters in the underlying process will be cut apart by the measuring window. In this connection, the cluster probability law estimated from short- T PNDs will be artificially skewed toward low cluster numbers and the rate of the primary process will accordingly appear to be larger than it really is. This problem is analogous to that of quadrat sampling for spatial processes in ecology. We should mention that the primary events need not be deterministic for the calculated value of $R(T)$ to be independent of stimulus level; the same result follows when the number of primary events is a Poisson random variable. This finding may be useful in interpreting PND data for noise stimuli. (For reproducible noise, of course, the number of primary events in the time T is deterministic.)

In short, it appears that although some of the details of the peripheral auditory neural point process remain elusive, many of the basic building blocks are in place. The Neyman-Scott cluster process provides us with a mathematical point of departure. In a future work, we will reconcile some of the theoretical distributions discussed here with our PND data.

IV. CONCLUSION

We have studied the pulse-number distribution (PND) for the extracellularly recorded nerve-spike train observed in primary afferent fibers in the auditory system of the cat. A broad range of pure-tone frequencies and intensity levels were used as stimuli, as was reproducible broadband Gaussian noise. High-, medium-, and low-spontaneous rate fibers,

with low and high characteristic frequencies, were examined. The counting time used in the work reported here was $T = 51.2$ ms. The spontaneous firing pattern of each unit was investigated by means of the PND, as well as the pulse-interval distribution (PID), and the twofold scaled PID. Data were simultaneously collected for the long-time ($T = 204.8$ ms) PND, and for the post-stimulus-time histogram (PST); the results of these studies will be reported at a future date.

Two unexpected observations emerged from our PND data: (i) the constancy of the count mean-to-variance ratio under a broad variety of conditions and (ii) the presence of spike clusters in the underlying VIIIth-nerve process. Our study has provided us with some important insights into the nature of cochlear nerve fiber events. A number of processes customarily used to model the auditory signal can be excluded. The cochlear neural point process is not a HPP, it is not an inhomogeneous PP, nor is it a DTMP, a DSPP with or without dead time, a RPP, or a simple binomial process. Rather, it appears to take the form of a cluster point process similar to the Neyman-Scott type. The PND can be expressed as a joint transformation of a multinomial random variable.

In the future, it will be useful to apply additional effort toward unraveling the details of the peripheral process by separating the various individual effects, so that their relative importance can be assessed. One way in which this task can be begun is to study the PND with different values of T . The key determinant of the information contained in the PND is the relationship of the counting time T to the correlation time of the process. If experiments can be conducted that exclude one or another of the constituent effects, while retaining the others, more can be learned about the coding mechanism. Refractory and simple synchrony effects in the PND should be more-or-less independent of T .

In addition, the behavior of the PND can be studied in various limits of the independent variables. Thus for \bar{n}/T small, dead-time effects become negligible [see Eq. (10)], whereas for M large, the simple synchrony effects described by Eq. (11) become negligible. It would appear, then, that the behavior of high-CF units firing at low rates should tell us about the point process in the absence of refractoriness and simple synchrony. In Fig. 13(a), we show the spontaneous PND for just such a unit [with $\bar{n} = 0.14$, $R(T = 51.2 \text{ ms}) = 0.82$]. This PND might be principally influenced by spike clusters.

It will, no doubt, also be useful to study the PND in conjunction with the PID, PST, and spectrum, for stimuli of various forms. Only by using all of the experimental tools at hand, and by eliminating theoretical models inconsistent with one or another aspect of the data, can we expect to increase our understanding of the underlying neural coding mechanisms. Our discussion has been centered about a single fiber. There is, of course, the enormously complex but exciting possibility of considering what happens when multiple fibers are involved (Johnson and Kiang, 1976). Several studies of this nature are now being conducted at higher centers in the auditory pathway (Gerstein *et al.*, 1983; Reitboeck, 1983; Abeles *et al.*, 1983).

ACKNOWLEDGMENTS

A great many people helped us with these experiments. Gary Sokolich sent us the designs for the probe microphone and sound-delivery system, and provided us with the probe-microphone calibration system. Jerry Palin designed a good deal of the electronics. Murray Sachs and Charles Liberman gave instruction in surgery and Debby Leonard and Martha Galley carried it out. Many undergraduate and graduate students wrote software and helped us conduct experiments: Sridhar Anandakrishnan, David Feld, Scott Halle, Ravi Khanna, Warren Morrow, Wayman Ng, Bob O'Connor, Gil Shuster, Ian Storper, Bob Turcott, and Faramak Wakil. Jont Allen, David Berkley, and Jim Flanagan of AT&T Bell Laboratories provided the computer hardware and an exceptional software base that enabled us to conduct our experiments. Finally, we received support from the National Institutes of Health under grant 2-R01-NS03654 and from the National Science Foundation under grant ECS82-19636.

APPENDIX A: SURGICAL PREPARATION

Healthy cats with clean external ears, weighing between 2.0 and 5.0 kg, were selected for the experiments. The animals were first given an intramuscular injection of chlorpromazine (14 mg per kg of body weight) and subsequently anesthetized with an intraperitoneal injection of sodium pentobarbital (Nembutal, 22 mg per kg of body weight). The anesthesia was maintained throughout the experiment by supplemental doses of pentobarbital (10% of the original dose at intervals of about 2 h). The cat was tracheotomized, the top of the skull was exposed, and a head holder was cemented to the skull using dental cement. This improved the mechanical stability in holding the skull. The bulla on the left side was opened and the septum was removed. A silver ball electrode was placed on the round window. A wire electrode was cemented to the bulla bone, anterior and superior to the round window location. A ground electrode was placed in the neck muscle. The cochlear microphonic signal was recorded differentially from the three electrodes. The ear canal was cut short to receive the ear insert used in delivering sound to the animal, and in measuring the sound pressure level near the tympanic membrane. The VIIIth nerve was accessed by means of a posterior Fossa approach (Kiang *et al.*, 1965). Finally, the cerebellum was retracted using cotton balls, and held in place by a metal retractor covered with cotton. The body temperature of the animal was monitored with a rectal thermometer. It was maintained between 37 °C and 39 °C throughout the course of the experiment, with the help of an Ealing heating blanket and temperature controller (see Fig. 2).

APPENDIX B: ACOUSTIC SIGNAL GENERATION

The acoustic signals used in our experiments were synthesized digitally by computer. Software was specially written for this purpose. As can be seen from Fig. 2, the digital signal (D) is converted to analog form by means of a digital-to-analog converter (D/A) and a programmable antialiasing filter (Rockland 816). Harmonic and intermodulation distortions in the signal are minimal (see Allen, 1983). The fre-

quency passband of the analog channels is roughly 65 Hz to 30 kHz. The high-frequency cutoff is presently limited by the D/A and analog-to-digital (A/D) hardware. The level of the acoustic signal applied to the cat is controlled in the two ways: (i) by specifying in software the output voltage of the D/A, and/or (ii) by computer control of a separate programmable voltage attenuator. Use of the programmable attenuator provides a higher signal-to-noise ratio (SNR) for the acoustic driver voltage at low levels. Part (a maximum of 40 dB) of the programmable attenuator is physically located in the amplifier; it is used when very low level signals are required. The output of the attenuator is applied to a push-pull amplifier that drives a balanced electrostatic transducer. This comprises the acoustic driver (Sokolich, 1977), which has a flat frequency response (± 3 dB) over a wide frequency range (65 Hz to 30 kHz). Its distortion levels at the highest output (90 dB SPL) are more than 60 dB below the fundamental level. The acoustic signal reaches the ear by means of a sound delivery tube which fits snugly into a truncated conical metal ear insert placed in the ear canal.

Aside from generating the digital acoustic signal in the manner described above, the computer simultaneously processes the idealized nerve spikes (N) from the cat and records data from two analog channels [the probe microphone (M) and the cochlear microphonic (C), each with a bandwidth of 30 kHz] on command. N, M, and C are schematically shown inside the oscilloscope block in Fig. 2.

APPENDIX C: ANALOG SIGNAL DETECTION AND PROCESSING

1. Sound pressure level measurement

The sound delivery tube has an angular bend, permitting a probe tube to be coaxially insert into it (see Fig. 2). The tip of the probe tube (Sokolich, 1977) reaches just beyond the edge of the ear insert, which is placed within about 5 mm of the tympanic membrane. The probe tube is attached to a Brüel and Kjaer (B&K 4134) 1/2-in. condenser microphone/cathode-follower system. The output is amplified using a compensating preamplifier (to adjust for the high-frequency rolloff of the probe tube). This signal is fed to the oscilloscope for monitoring and, through an antialiasing filter and an A/D converter, to the computer for recording on command. The amplified signal produced by the probe microphone (M) is noisy because of the weak acoustic signals being measured at low stimulus levels. Its SNR is therefore enhanced by synchronously averaging for 50 frames of response. The averaging is carried out by accumulating the signal in 2048 time bins, each of 25- μ s width, for the range of pure-tone frequencies applied to the ear. The fundamental component of the signal is then extracted from the averaged data by a fast Fourier transform (FFT) routine. The probe microphone is calibrated prior to the experiment by using a test cavity designed by Sokolich (personal communication, 1976). The probe calibration is used to correct the measured sound pressure to yield the absolute sound pressure level (SPL) at the tympanic membrane for a fixed electrical voltage applied to the acoustic driver. After the initial calibration, the SPL may be determined directly from the probe microphone response or it may alternatively be inferred

from the electrical voltage applied to the acoustic transducer.

2. CM measurement

The round window (RW) cochlear microphonic (CM) is used to monitor the condition of the cochlea. The CM voltage is measured differentially between the RW, bulla bone, and ground electrodes (see Fig. 2). A PARC 113 differential amplifier, with a gain of 5000, is used to amplify the signal. The output (C) is monitored on the oscilloscope and fed to the computer for recording on command, via an antialiasing filter and an A/D converter. To improve the SNR of the CM response, signals are accumulated in 2048 25- μ s time bins, for 50 repetitions, and averaged by the computer. Again, the FFT routine is used to extract the amplitude and phase of the fundamental component of the response. Round-window CM responses are recorded for the frequency range from 65 Hz to 30 kHz, in increments of 100 Hz. A fixed electrical input to the transducer is maintained while measuring each CM curve. A family of CM curves is obtained by decreasing the electrical input to the acoustic transducer in 10-dB steps. Five different levels are usually recorded. These CM plots are repeated periodically throughout the course of the experiment and compared with the initial set, to signal any changes in the condition of the animal's auditory system.

APPENDIX D: NEURAL SIGNAL DETECTION AND PROCESSING

Selected glass microelectrodes filled with 3 M KCl (with resistances in the range 5–30 M Ω), are held in a plastic electrode holder. They are positioned with respect to the animal with the help of an x-y-z micromanipulator. After placing the microelectrode near the VIIIth nerve, with its tip in the cerebrospinal fluid (CSF), the electrode impedance is determined. The precise position and direction at which the electrode is directed to penetrate the nerve is determined by the desired values of the characteristic frequencies (CF) for the experiment at hand.

The electrical output of the microelectrode is amplified by means of a high-input-impedance negative-capacitance compensation amplifier, followed by a PARC 113 low-noise preamplifier (see Fig. 2). The neural signal (S) is displayed on the oscilloscope for visual monitoring, and simultaneously fed to a loudspeaker, for acoustic monitoring of the nerve spikes. It is also sent to a level discriminator that produces standardized 1- μ s-duration impulses each time the neural signal exceeds a manually adjustable preset threshold. Spikes are electronically prohibited from being closer to each other than 0.95 ms (electronic dead time) to avoid inadvertent double triggering on a single nerve spike. Only a few percent of the events occur within a time shorter than 0.95 ms (Littlefield, 1973) so that the data is not seriously altered. We have experimentally examined the effect of this dead time in some detail and demonstrated explicitly that it is small. The idealized neural spikes (N) are also displayed on the oscilloscope and recorded by the computer using special histogram hardware [see Allen (1983) for details]. An assembly language program (BHIST) enabled us to reset the histogram counter either by means of the unused least significant

bit (LSB) of the real-time D/A word (for the PND and PST), or by the arrival of a subsequent neural spike (for the PIDs).

In conducting an experiment, the microelectrode is advanced into the nerve by means of a Burleigh "inchworm" piezoelectric micropositioner with a remote controller. A position sensor on the inchworm device indicates the depth of the electrode. When the microelectrode just touches the nerve sheath, the depth counter is set to zero, and gated wideband noise is applied to the cat's ear by the acoustic driver. The electrode is advanced in 2- μ m steps. Bursts of neural activity from the loudspeaker, synchronized with the 1-s gated noise, signal the acquisition of an auditory unit. The electrode is then left in position, the noise is turned off, and the neural-threshold rate frequency tuning curve (FTC) of the unit is determined. [The FTC is computed in accordance with an algorithm reported by Kiang *et al.* (1970), and by Liberman (1978). The use of this algorithm in our system has been discussed by Allen (1983)]. In a typical preparation, units are encountered roughly 50 μ m apart. After about 2000 μ m of electrode travel, it is withdrawn and repositioned. The electrode is then advanced again in the manner described above.

- Abbas, P. J., and Sachs, M. B. (1976). "Two-tone suppression in auditory-nerve fibers: Extension of a stimulus-response relationship," *J. Acoust. Soc. Am.* **59**, 112–122.
- Abeles, M., de Ribaupierre, F., and de Ribaupierre, Y. (1983). "Detection of single unit responses which are loosely time-locked to a stimulus," *IEEE Trans. Syst. Man Cybern.* **SMC-13**, 683–691.
- Allen, J. B. (1983). "Magnitude and phase-frequency response to single tones in the auditory nerve," *J. Acoust. Soc. Am.* **73**, 2071–2092.
- Anderson, D. J. (1973). "Quantitative model for the effects of stimulus frequency on synchronization of auditory nerve discharges," *J. Acoust. Soc. Am.* **54**, 361–364.
- Barlow, H. B., and Levick, W. R. (1969a). "Three factors limiting the reliable detection of light by the retinal ganglion cells of the cat," *J. Physiol. (London)* **200**, 1–24.
- Barlow, H. B., and Levick, W. R. (1969b). "Changes in the maintained discharge with adaptation level in the cat retina," *J. Physiol. (London)* **202**, 699–718.
- Barlow, H. B., Levick, W. R., and Yoon, M. (1971). "Responses to single quanta of light in retinal ganglion cells of the cat," *Vision Res.* **11** (Suppl. 3), 87–101.
- Brink, F., Jr., Bronk, D. W., and Larabee, M. G. (1946). "Chemical excitation of a nerve," *Ann. NY Acad. Sci.* **47**, 457–485.
- Cantor, B. I., and Teich, M. C. (1975). "Dead-time-corrected photocounting distributions for laser radiation," *J. Opt. Soc. Am.* **65**, 786–791.
- Cox, D. R. (1962). *Renewal Theory* (Methuen, London, England).
- Cox, D. R., and Isham, V. (1980). *Point Processes* (Chapman and Hall, London, England).
- Cox, D. R., and Lewis, P. A. W. (1966). *The Statistical Analysis of Series of Events* (Methuen, London, England).
- de Kwaadsteniet, J. W. (1982). "Statistical analysis and stochastic modeling of neuronal spike-train activity," *Math. Biosci.* **60**, 17–71.
- Einstein, A. (1909). "Zum gegenwärtigen Stand des Strahlungsproblems," *Phys. Z.* **10**, 185–193.
- Ekhholm, A. (1972). "A generalization of the two-state two-interval semi-Markov model," in *Stochastic Point Processes: Statistical Analysis, Theory, and Applications*, edited by P. A. W. Lewis (Wiley-Interscience, New York), pp. 272–284.
- Ekhholm, A., and Hyvärinen, J. (1970). "Computer simulation of the impulse pattern of muscle spindle afferents under static and dynamic conditions," *Kybernetik (Biol. Cybern.)* **10**, 171–178.
- Evans, E. F. (1972). "The frequency response and other properties of single fibers in the guinea-pig cochlear nerve," *J. Physiol. (London)* **226**, 263–287.

- Evans, E. F. (1975). "Cochlear nerve and cochlear nucleus," in *Handbook of Sensory Physiology, Vol. V/2, Auditory System*, edited by W. D. Keidel and W. D. Neff (Springer-Verlag, Berlin), pp. 1-108.
- Fienberg, S. E. (1974). "Stochastic models for single neuron firing trains: A survey," *Biometrics* 30, 399-427.
- Galambos, R., and Davis, H. (1943). "The response of single auditory nerve fibers to acoustic stimulation," *J. Neurophysiol.* 6, 39-57.
- Galambos, R., and Davis, H. (1948). "Action potentials from single auditory fibers?," *Science* 108, 513.
- Gaumont, R. P., Molnar, C. E., and Kim, D. O. (1982). "Stimulus and recovery dependence of cat cochlear nerve fiber spike discharge probability," *J. Neurophysiol.* 48, 856-873.
- Gerstein, G. L., Blöom, M. J., Espinosa, I. E., Evanczuk, S., and Turner, M. R. (1983). "Design of a laboratory for multineuron studies," *IEEE Trans. Syst. Man Cybern.* SMC-13, 668-676.
- Gerstein, G. L., and Kiang, N. Y-S. (1960). "An approach to the quantitative analysis of electrophysiological data from single neurons," *Biophys. J.* 1, 15-28.
- Gerstein, G. L., and Mandelbrot, B. (1964). "Random walk models for the spike activity of a single neuron," *Biophys. J.* 4, 41-68.
- Goldberg, J. M., and Brown, P. B. (1969). "Response of binaural neurons of dog superior olivary complex to dichotic tonal stimuli: Some physiological mechanisms of sound localization," *J. Neurophysiol.* 32, 613-636.
- Gray, P. R. (1967). "Conditional probability analysis of the spike activity of single neurons," *Biophys. J.* 7, 759-777.
- Gundersdorf, C. J. (1971). "A new method for determining some statistical properties of light," in *Quantum Limitations on Optical Communications* (John Hopkins Univ., Carlyle Barton Lab., Baltimore, MD), Tech. Rep. no. AFAL-TR-71-58, DDC no. AD882879, pp. 76-175.
- Hagiwara, S. (1954). "Analysis of interval fluctuation of the sensory nerve impulse," *Jpn. J. Physiol.* 4, 234-240.
- Haight, F. A. (1967). *Handbook of the Poisson Distribution* (Wiley, New York).
- Hecht, S., Shlaer, S., and Pirenne, M. H. (1942). "Energy, quanta and vision," *J. Gen. Physiol.* 25, 819-840.
- Hind, J. E., Anderson, D. J., Brugge, J. F., and Rose, J. E. (1967). "Coding of information pertaining to paired low-frequency tones in single auditory nerve fibers of the squirrel monkey," *J. Neurophysiol.* 30, 794-816.
- Holden, A. V. (1976). "Models of the stochastic activity of neurones," in *Lecture Notes in Biomathematics*, edited by S. Levin (Springer-Verlag, Berlin), Vol. 12.
- Holden, A. V., and Winlow, W. (1983). "Neuronal activity as the behavior of a differential system," *IEEE Trans. Syst. Man Cybern.* SMC-13, 711-719.
- Hyvärinen, J. (1966). "Analysis of spontaneous spike potential activity in developing rabbit diencephalon," *Acta Physiol. Scand.* 68, Suppl. 278.
- Javel, E., Geisler, C. D., and Ravindran, A. (1978). "Two-tone suppression in auditory nerve of the cat: Rate-intensity and temporal analyses," *J. Acoust. Soc. Am.* 63, 1093-1104.
- Johnson, D. H. (1978). "The relationship of post-stimulus time and interval histograms to the timing characteristics of spike trains," *Biophys. J.* 22, 413-430.
- Johnson, D. H. (1980). "The relationship between spike rate and synchrony in responses of auditory-nerve fibers to single tones," *J. Acoust. Soc. Am.* 68, 1115-1122.
- Johnson, D. H., and Kiang, N. Y-S. (1976). "Analysis of discharges recorded simultaneously from pairs of auditory nerve fibers," *Biophys. J.* 16, 719-734.
- Johnson, D. H., and Swami, A. (1983). "The transmission of signals by auditory-nerve fiber discharge patterns," *J. Acoust. Soc. Am.* 74, 493-501.
- Katsuki, Y., Sumi, T., Uchiyama, H., and Watanabe, T. (1958). "Electric responses of auditory neurones in cat to sound stimulation," *J. Neurophysiol.* 21, 569-588.
- Kiang, N. Y-S. (1984). "Peripheral neural processing of auditory information," in *Handbook of Physiology: The Nervous System, Vol. 3, Sensory Processes*, edited by I. Darian Smith (Am. Physiol. Soc., Bethesda, MD), pp. 639-674.
- Kiang, N. Y-S., Baer, T., Marr, E. M., and Demont, D. (1969). "Discharge rates of single auditory-nerve fibers as functions of tone level," *J. Acoust. Soc. Am.* 46(A), 106.
- Kiang, N. Y-S., and Moxon, E. (1972). "Physiological considerations in artificial stimulations of the inner ear," *Ann. Otol. Rhinol. Laryngol.* 81, 714-730.
- Kiang, N. Y-S., Moxon, E. C., and Levine, R. A. (1970). "Auditory-nerve activity in cats with normal and abnormal cochleas," in *Sensorineural Hearing Loss*, edited by G. E. W. Wolstenholme and J. Knight (Churchill, Great Britain), pp. 241-273.
- Kiang, N. Y-S., Watanabe, T., Thomas, E. C., and Clark, L. F. (1962). "Stimulus coding in the cat's auditory nerve," *Ann. Otol. Rhinol. Laryngol.* 71, 1009-1026.
- Kiang, N. Y-S., Watanabe, T., Thomas, E. C., and Clark, L. F. (1965). *Discharge Patterns of Single Fibers in the Cat's Auditory Nerve*, Res. Monogr. no. 35 (MIT, Cambridge, MA).
- Kuffler, S. W., FitzHugh, R., and Barlow, H. B. (1957). "Maintained activity in the cat's retina in light and darkness," *J. Gen. Physiol.* 40, 683-702.
- Landolt, J. P., and Correia, M. J. (1978). "Neuromathematical concepts of point process theory," *IEEE Trans. Biomed. Eng.* BME-25, 1-12.
- Lewis, P. A. W. (1972). "Recent results in the statistical analysis of univariate point processes," in *Stochastic Point Processes: Statistical Analysis, Theory, and Applications*, edited by P. A. W. Lewis (Wiley-Interscience, New York), pp. 1-54.
- Lieberman, M. C. (1978). "Auditory-nerve response from cats raised in a low-noise chamber," *J. Acoust. Soc. Am.* 63, 442-455.
- Lieberman, M. C. (1983). Personal communication.
- Littlefield, W. M. (1973). "Investigation of the linear range of the peripheral auditory system," Ph.D. thesis, Department of Electrical Engineering, Washington Univ., St. Louis, MO.
- Littlefield, W. M., Pfeiffer, R. R., and Molnar, C. E. (1972). "Modulation index as a response criterion for discharge activity," *J. Acoust. Soc. Am.* 51, 93.
- Lütkenhöner, B., Hoke, M., and Bappert, E. (1980). "Influence of refractory properties on the response of single auditory nerve fibers to sinusoidal stimuli," *Hear. Res.* 2, 565-572.
- Mandel, L. (1959). "Fluctuations of photon beams: The distribution of the photo-electrons," *Proc. Phys. Soc. (London)* 74, 233-243.
- McGee, J., Farley, G. R., Walsh, E. J., and Javel, E. (1981). "High-intensity 'notches' in responses of auditory nerve fibers," *J. Acoust. Soc. Am. Suppl.* 1 69, S53.
- McGill, W. J. (1967). "Neural counting mechanisms and energy detection in audition," *J. Math. Psychol.* 4, 351-376.
- Moore, G. P., Perkel, D. H., and Segundo, J. P. (1966). "Statistical analysis and functional interpretation of neuronal spike data," *Ann. Rev. Physiol.* 28, 493-522.
- Müller, J. W. (1973). "Dead-time problems," *Nucl. Instrum. Methods* 112, 47-57.
- Müller, J. W. (1974). "Some formulae for a dead-time-distorted Poisson process," *Nucl. Instrum. Methods* 117, 401-404.
- Neyman, J., and Scott, E. L. (1958). "A statistical approach to problems of cosmology," *J. R. Stat. Soc. Ser. B* 20, 1-43.
- Parzen, E. (1962). *Stochastic Processes* (Holden-Day, San Francisco, CA), pp. 117-186.
- Peake, W. T., Goldstein, M. H., Jr., and Kiang, N. Y-S. (1962). "Responses of the auditory nerve to repetitive acoustic stimuli," *J. Acoust. Soc. Am.* 34, 562-570.
- Pecher, C. (1939). "La fluctuation d'excitabilité de la fibre nerveuse," *Arch. Intern. Physiol.* 49, 129-152.
- Perkel, D. H., Gerstein, G. L., and Moore, G. P. (1967). "Neuronal spike trains and stochastic point processes. I. The single spike train," *Biophys. J.* 7, 391-418.
- Prucnal, P. R., and Teich, M. C. (1983). "Refractory effects in neural counting processes with exponentially decaying rates," *IEEE Trans. Syst. Man Cybern.* SMC-13, 1028-1033.
- Reitboeck, H. J. P. (1983). "A 19-channel matrix drive with individually controllable fiber microelectrodes for neurophysiological applications," *IEEE Trans. Syst. Man Cybern.* SMC-13, 676-683.
- Ricciardi, L. M., and Esposito, F. (1966). "On some distribution functions for non-linear switching elements with finite dead time," *Kybernetik (Biol. Cybern.)* 3, 148-152.
- Rodieck, R. W., Kiang, N. Y-S., and Gerstein, G. L. (1962). "Some quantitative methods for the study of spontaneous activity of single neurons," *Biophys. J.* 2, 351-368.
- Rose, J. E., Brugge, J. F., Anderson, D. J., and Hind, J. E. (1967). "Phase-locked response to low frequency tones in single auditory nerve fibers of the squirrel monkey," *J. Neurophysiol.* 30, 769-793.
- Rose, J. E., Hind, J. E., Anderson, D. J., and Brugge, J. F. (1971). "Some effects of stimulus intensity on response of auditory nerve fibers in the squirrel monkey," *J. Neurophysiol.* 34, 685-699.
- Ruggero, M. A. (1973). "Response to noise of auditory nerve fibers in the squirrel monkey," *J. Neurophysiol.* 36, 569-587.
- Ruggero, M. A., and Rich, N. C. (1983). "Chinchilla auditory nerve re-

- sponses to low-frequency tones," *J. Acoust. Soc. Am.* **73**, 2096–2108.
- Rupert, A., Moushegian, G., and Galambos, R. (1963). "Unit responses to sound from auditory nerve of the cat," *J. Neurophysiol.* **26**, 449–465.
- Rutherford, W. (1886). "A new theory of hearing," *J. Anat. Physiol.* **21**, 166–168.
- Rutherford, E., and Geiger, H. (1910). "The probability variation in the distribution of α particles," *Philos. Mag.* **20**, 698–707.
- Saleh, B. E. A. (1978). *Photoelectron Statistics* (Springer-Verlag, Berlin).
- Saleh, B. E. A., and Teich, M. C. (1982). "Multiplied-Poisson noise in pulse, particle, and photon detection," *Proc. IEEE* **70**, 229–245.
- Siebert, W. M. (1968). "Stimulus transformations in the peripheral auditory system," in *Recognizing Patterns*, edited by P. A. Kolars and M. Eden (MIT, Cambridge, MA), pp. 104–133.
- Snyder, D. (1975). *Random Point Processes* (Wiley-Interscience, New York).
- Sokolich, W. G. (1976). Personal communication.
- Sokolich, W. G. (1977). "Improved acoustic system for auditory research," *J. Acoust. Soc. Am. Suppl.* **1** **62**, S12.
- Sugano, N. (1983). "Effect of doublet impulse sequences in the crayfish claw opener muscles and the computer-simulated neuromuscular synapse," *Biol. Cybern.* **49**, 55–61.
- Tasaki, I. (1954). "Nerve impulses in individual auditory nerve fibers of guinea pig," *J. Neurophysiol.* **17**, 97–122.
- Teich, M. C., and Diamant, P. D. (1980). "Relative refractoriness in visual information processing," *Biol. Cybern.* **38**, 187–191.
- Teich, M. C., and Khanna, S. M. (1982). "Pulse-number distribution for the neural discharge in the cat's auditory nerve," *J. Acoust. Soc. Am. Suppl.* **1** **71**, S17.
- Teich, M. C., and Khanna, S. M. (1983). "Behavior of the pulse-number distribution for the neural spike train in the cat's auditory nerve," *J. Acoust. Soc. Am. Suppl.* **1** **74**, S7.
- Teich, M. C., and Lachs, G. (1979). "A neural-counting model incorporating refractoriness and spread of excitation. I. Application to intensity discrimination," *J. Acoust. Soc. Am.* **66**, 1738–1749.
- Teich, M. C., Matin, L., and Cantor, B. I. (1978). "Refractoriness in the maintained discharge of the cat's retinal ganglion cell," *J. Opt. Soc. Am.* **68**, 386–402.
- Teich, M. C., and McGill, W. J. (1976). "Neural counting and photon counting in the presence of dead time," *Phys. Rev. Lett.* **36**, 754–758.
- Teich, M. C., Prucnal, P. R., Vannucci, G., Breton, M. E., and McGill, W. J. (1982). "Multiplication noise in the human visual system at threshold: I. Quantum fluctuations and minimum detectable energy," *J. Opt. Soc. Am.* **72**, 419–431.
- Teich, M. C., and Saleh, B. E. A. (1981). "Interevent-time statistics for shot-noise-driven self-exciting point processes in photon detection," *J. Opt. Soc. Am.* **71**, 771–776.
- Teich, M. C., Saleh, B. E. A., and Pefina, J. (1984). "Role of primary excitation statistics in the generation of antibunched and sub-Poisson light," *J. Opt. Soc. Am. B* **1**, 366–389.
- Ten Hoopen, M., Den Hertog, A., and Reuver, H. A. (1963). "Fluctuation in excitability of nerve fibers—A model study," *Kybernetik (Biol. Cybern.)* **2**, 1–8.
- Vannucci, G., and Teich, M. C. (1978). "Effects of rate variation on the counting statistics of dead-time-modified Poisson processes," *Opt. Commun.* **25**, 267–272.
- Verveen, A. A. (1961). *Fluctuation in Excitability* (Drukkerij Holland, Amsterdam, The Netherlands).
- Walsh, B. T., Miller, J. B., Gacek, R. R., and Kiang, N. Y-S. (1972). "Spontaneous activity in the eighth cranial nerve of the cat," *Int. J. Neurosci.* **3**, 221–236.
- Weiss, T. F. (1966). "A model of the peripheral auditory system," *Kybernetik (Biol. Cybern.)* **3**, 153–175.